Title
MEASUREMENT OF THE N*- - N*++ MASS DIFFERENCE

Author
Kim, Sedong.

Publication Date
1965-07-01

UCRL-16189 (corrected)

University of California

Ernest O. Lawrence Radiation Laboratory

MEASUREMENTS OF THE $N^{*-} - N^{*++}$ MASS DIFFERENCE

Berkeley, California

DISCLAIMER

UNIVERSITY OF CALIFORNIA

Lawrence Radiation Laboratory
Berkeley, California

November 4, 1965

ERRATA

TO: All recipients of UCRL-16189

FROM: Technical Information Division

Subject: UCRL-16189, Measurement of the $N^{*-} - N^{*++}$ Mass Difference
July 1965 (Sedong Kim, Ph. D. Thesis)

Please make the following corrections on subject report.

Replace pages 1-2 with the attached.

done

Research and Development

UCRL-16189

UNIVERSITY OF CALIFORNIA
Lawrence Radiation Laboratory
Berkeley, California

AEC Contract No. W-7405-eng-48

MEASUREMENT OF THE $N^{*-} - N^{*++}$ MASS DIFFERENCE

Sedong Kim
(Ph. D. Thesis)

July 1965

MEASUREMENT OF THE N^{*-} - N^{*++} MASS DIFFERENCE

Contents

MEASUREMENT OF THE N^{*-} - N^{*++} MASS DIFFERENCE

Sedong Kim

Lawrence Radiation Laboratory
University of California
Berkeley, California

ABSTRACT

A measurement of the mass and width difference between N^{*-} ($I_Z = -3/2$) and N^{*++} ($I_Z = +3/2$) is described, where N^* is the pion-nucleon p-wave resonance of spin and isotopic spin 3/2 and mass approximately 1240 MeV. The resonances were produced in the inelastic reactions $n\ n \rightarrow p\ n\ \pi^-$ and $p\ p \rightarrow n\ p\ \pi^+$, which are known to proceed almost entirely via N^{*-} and N^{*++} production, respectively, in the observed energy region of a few BeV. The masses and widths of N^{*-} and N^{*++} were obtained from their respective effective mass distributions. In fitting the data for the masses we used two different formulae: a) the OPE (one-pion-exchange) formula and b) the resonance formula, with constant matrix element, which goes according to the phase space. Because the above inelastic reactions are known to be dominated by OPE, the values obtained with the OPE formula are taken to be the best estimate of the resonance parameters. This gives a mass difference of $\delta\omega_o = N^{*-} - N^{*++} = 7.9 \pm 6.8$ MeV and a width difference of $\delta\Gamma_o = 25 \pm 23$ MeV. This result agrees with the predictions based on the SU(3) and SU(6) symmetry schemes and various dynamical theories.

I. INTRODUCTION

The nucleon-pion system has a resonant state known as the (3,3) resonance or the $N^*_{3/2}$, having isotopic spin I = 3/2, angular momentum J = 3/2, and orbital angular momentum $\ell = 1$. This resonance was first discovered by Anderson, Fermi and collaborators at Chicago[1] in 1953 in the elastic reaction $\pi^+ p \rightarrow \pi^+ p$, and was the first resonance to be discovered between two strongly interacting particles. The cross-section for $\pi^+ p \rightarrow \pi^+ p$ showed a very pronounced peak at the π^+ laboratory kinetic energy of about 200 MeV, corresponding to the resonance mass of around 1240 MeV. Subsequently, the resonance was also observed in other scattering experiments: $\pi^- p \rightarrow \pi^- p$ and $\pi^- p \rightarrow \pi^o n$; and in photoreactions $\gamma p \rightarrow p \pi^o$ and $\gamma p \rightarrow n \pi^+$, establishing N^{*++}, N^{*+}, N^{*o} and N^{*-} as the members of the N^* isomultiplet. This resonance also occurs in the inelastic processes such as $\pi N \rightarrow N \pi\pi$ and $N N \rightarrow N N \pi$. In the inelastic reactions the resonance shows up as a peak in the invariant mass plot of its component particles (N and π).

In the SU(3) symmetry scheme[2] N^* is a member of the $J^P = 3/2^+$ decuplet, along with Y^*, Ξ^*, and Ω^- (Fig. 1). Okubo[3] has recently pointed out that, because of electromagnetic mass splitting, the Gell-Mann-Okubo[2] mass formula is valid only for particles with the same charge. {In general,[3] $\Delta M = a_o + a_1 Y + a_2 [1/4\, Y^2 - I(I+1)] + b_1 Q + b_2 [1/4\, Q^2 - U(U+1)] + b_3 Q^2 + b_4 Q [1/4\, Q^2 - U(U+1)] + b_5 [1/4\, Q^2 - U(U+1)]^2$, where a's and b's are constants, Y and I are hypercharge and I spin, and Q and U, charge and U spin, respectively. Here Y = S + B, where S stands for the strangeness and B is the baryon number. U multiplets have (2U + 1) components corresponding to the different U_Z of the same charge.} In particular, a knowledge of the N^{*-} is required for the

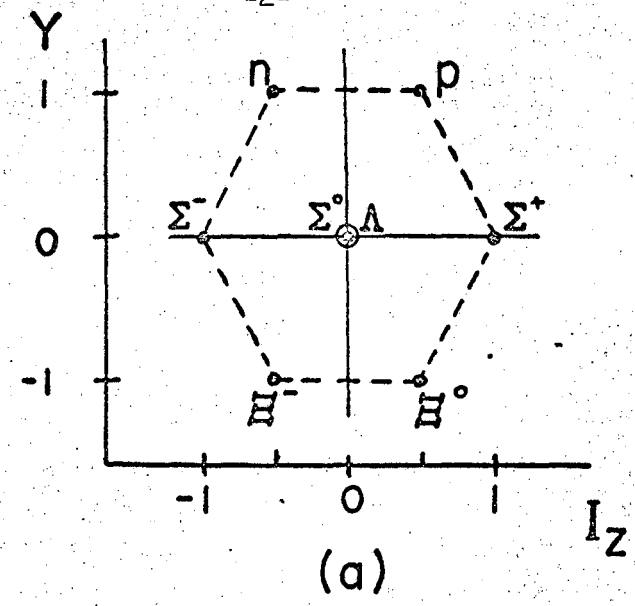

(a)

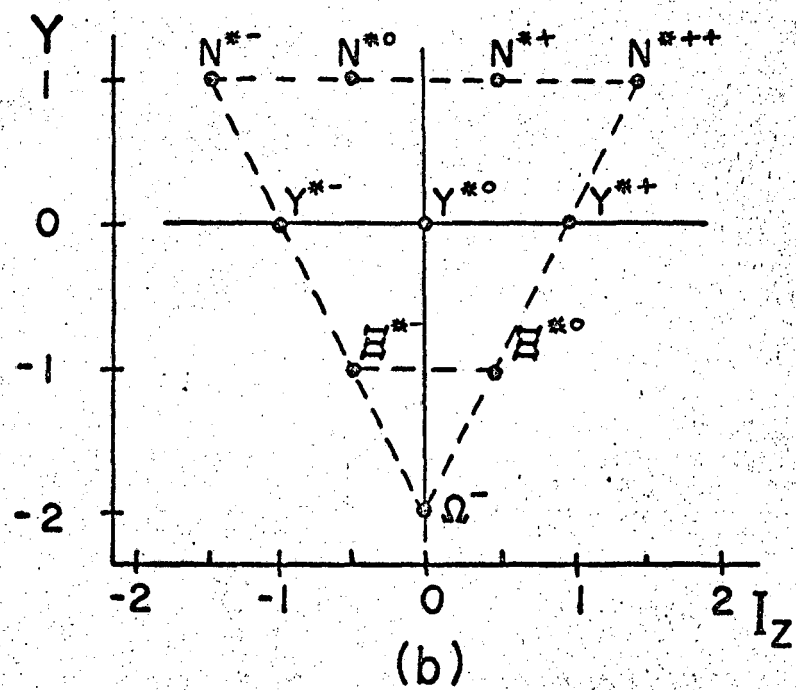

(b)

Fig. 1

comparison $\Omega^- - \Xi^{*-} = \Xi^{*-} - Y^{*-} = Y^{*-} - N^{*-}$ (The particle symbol represents its mass.). The decay width of N^{*-} is also needed to test the predicted relationship between the decay amplitudes of the decuplet particles Ξ^*, Y^*, and N^* .[4] In addition, the measured mass difference can be compared with the predictions of the various symmetry schemes.

The masses of particles within a given SU(2) representation are believed to be identical in the limit of isotopic spin invariance. The electromagnetic force removes this degeneracy, giving rise to mass differences of the order of $\alpha\, m_\pi$ (α is the fine-structure constant). In principle, the mass differences within an isomultiplet are obtainable by a calculation of the electromagnetic self-energies of the particles therein. The attempts to calculate self-energies for strongly interacting particles, within the framework of a perturbative expansion of field theory, have been unsuccessful.

In the unitary symmetry scheme isomultiplets of different hypercharge are grouped into "supermultiplets" (or unitary multiplets) which form the irreducible representations of the SU(3) group. It is postulated that, in the limit of exact unitary symmetry, the masses of all particles within a given SU(3) representation are identical. The observed mass differences between isomultiplets within a unitary multiplet are of the order of 100 MeV, and are believed to arise from the "medium-strong" force. By making the assumption that unitary symmetry is violated only by the electromagnetic interaction, it is possible to relate the mass splittings within different isomultiplets of a supermultiplet. In the baryon octet, for example, the prediction[5] of $\Xi^- - \Xi^o = \Sigma^- - \Sigma^+ + p - n$ has been experimentally confirmed.[6] For the $3/2^+$ decuplet, of which N^* is a member, the relationship

$$\Delta M = a + bQ + cQ^2$$

is predicted (from Gell-Mann-Okubo mass formula and the relations U = 1 - 1/2 Q and I = 1 + 1/2 Y), where Q is the charge and a, b, and c are constants.[7] This gives the following relations among the members of the decuplet:

$$N^{*+} - N^{*0} = Y^{*+} - Y^{*0} = 1/3\,[N^{*++} - N^{*-}]$$

and $$N^{*0} - N^{*-} = Y^{*0} - Y^{*-} = \Xi^{*0} - \Xi^{*-}.$$

Coleman and Glashow have noted that the mass splittings within an SU(3) supermultiplet follow an octet pattern, and have proposed a dynamical theory of unitary symmetry violation, namely that symmetry-breaking processes are dominated by "tadpole" diagrams because of the existence of an octet of scalar mesons.[8] For the $3/2^+$ decuplet such an octet dominance leads to an "equal-spacing" rule for electromagnetic splitting,

$$N^{*++} - N^{*+} = N^{*+} - N^{*0} = N^{*0} - N^{*-}$$
$$= Y^{*+} - Y^{*0} = Y^{*0} - Y^{*-} = \Xi^{*0} - \Xi^{*-}.$$

It also gives an intramultiplet relationship

$$\frac{N^{*++} - N^{*+}}{N^{*} - Y^{*}} = \frac{\Sigma^{+} - \Sigma^{-}}{N - \Xi}$$

which yields $N^{*++} - N^{*+} = -3.0$ MeV and $N^{*+} - N^{*-} = -9.1$ MeV. These predictions must, however, be modified by the contributions of other mass-splitting diagrams. The leading nontadpole contribution to the electromagnetic self-masses of baryons comes from intermediate states containing one baryon and one photon.[9] The tadpole and nontadpole contributions to the electromagnetic mass differences are shown in Table I.

Dashen and Frautschi have proposed a bootstrap mechanism to explain octet dominance of the mass splitting.[10] Higher-order effects in this model again reduce the splitting and alter the equal-spacing pattern.

The group SU(6) contains both SU(2) and SU(3) as subgroups. In the recently proposed SU(6) symmetry scheme the baryon octet and the $J^P = 3/2^+$ decuplet are assigned to the 56-dimensional representation of SU(6).[11] The relations between the 10 mass differences in the 56 representation have been derived in the limit where SU(6) symmetry is broken by electromagnetism only:[12]

$$\Xi^- - \Xi^0 = (\Sigma^- - \Sigma^+) - (n - p),$$

$$N^{*0} - N^{*+} = Y^{*0} - Y^{*+} = n - p,$$

$$N^{*-} - N^{*0} = Y^{*-} - Y^{*0} = \Xi^{*-} - \Xi^{*0}$$

$$= (n - p) + (\Sigma^- + \Sigma^+ - 2\Sigma^0),$$

$$N^{*-} - N^{*++} = 3(n - p).$$

The relationships among the decuplet members are identical with the SU(3) predictions.

Mass differences between various members of isomultiplets are needed to test the above mass formulae. The $N^{*-} - N^{*++}$ seems to be the pair which is most sensitive to electromagnetic mass splitting in the N^* isomultiplet. In this experiment we measure the mass difference $N^{*-} - N^{*++}$, in order to check some of the above mass formulae. In section II, we discuss the experimental details, such as the beam layout, the selection of events and the method of data analysis. In section III possible systematic errors are considered. In section IV we discuss the one-pion-exchange model in connection with this experiment. In section V we present the results and discuss the problem of elucidating resonance parameters from plots of invariant mass. Finally, in section VI we compare the experimental measurement with predictions based on the SU(3) and SU(6) symmetry schemes.

II. EXPERIMENTAL DETAILS

A. Beam Geometry

In this experiment, the 20-inch bubble chamber filled with deuterium (.0688 gm/cc) was exposed to a beam of 3.64 BeV/c separated deuterons at the alternating-gradient synchrotron (AGS) of Brookhaven National Laboratory.

The beam layout[13] is shown in Fig. 2. The first stage consists of the transport section which demagnifies the target, focusing the image on slit 2, which then serves as a source for the remaining part of the beam. It also gives a rough momentum determination for the beam. The next two stages are composed of velocity spectrometers BS1 and BS2, and the associated quadrupole optics. Slit 3 at the end of the first separation stage is the mass resolution slit. Precise momentum definition is obtained at the beginning of the second separation stage by virtue of a large-angle deflection of the beam. Slit 4 serves as a momentum-defining and mass-resolution slit. The beam-shaping section in the final stage shapes the image to fill the chamber.

The BNL 20-inch bubble chamber[14] has an illuminated volume of about 19 inches in the beam direction by 8 inches high by 10 inches deep. Its total liquid volume is 60 liters. It was operated in a magnetic field of 17,000 gauss. The field varied by less than 3% over the chamber volume. A total of 20,000 pictures with four stereo views were taken.

B. Selection of Events

The resonances were produced in the inelastic reactions

$$n\ n \rightarrow p_1\ n_2\ \pi_3^- \qquad (1)$$

$$p\ p \rightarrow n_1\ p_2\ \pi_3^+ \qquad (2)$$

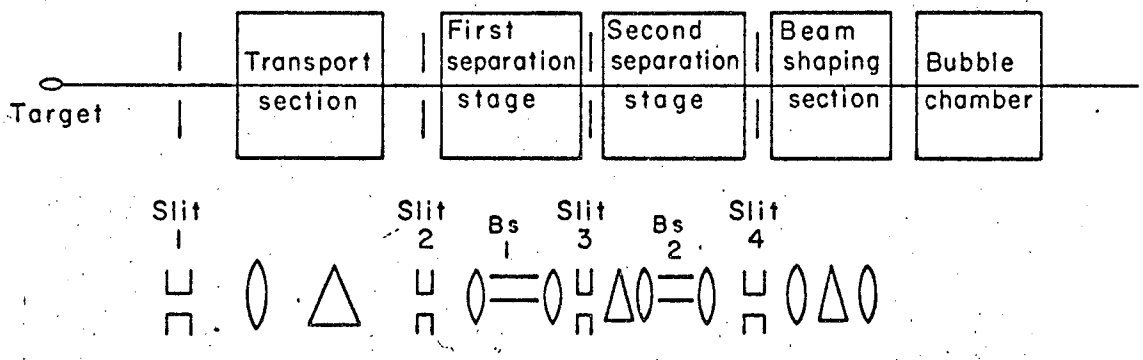
Target
Transport section
First separation stage
Second separation stage
Beam shaping section
Bubble chamber
Slit 1
Slit 2
Bs 1
Slit 3
Bs 2
Slit 4
MU-32298

Fig. 2

at a mean C. M. energy of 2.35 BeV. At this energy reactions (1) and (2) are known to proceed almost entirely via N^{*-} and N^{*++} production, respectively. We determined the mass difference, $\delta\omega_o$, and the width difference, $\delta\Gamma_o$, by a comparison of the distributions in the invariant mass, ω_{23}, for both reactions.

Two conditions are desirable to achieve a precise measurement:

(a) Reactions (1) and (2) should occur under identical experimental conditions.

(b) Both reactions should occur at the same energy.

Condition (b) is necessary because the shape of the invariant-mass plot depends on the production mechanism, and a quantitative description of the production mechanism as a function of energy is not available. By observing N^* production in charge-symmetric reactions at the same energy, one insures that any difference in the invariant-mass plots is due to electromagnetic effects only.

In this experiment the two reactions were simultaneously achieved at the same energy and under identical experimental conditions by the interactions of a beam of deuterons with deuterium in the bubble chamber. In the majority of d-d collisions one nucleon in each deuteron is a spectator. Reactions (1) and (2) occured in the interactions

$$d\,d \rightarrow p_S^T\, p_S^B\, p_1\, n_2\, \pi_3^- \qquad (1a)$$

$$\text{and } d\,d \rightarrow n_S^T\, n_S^B\, n_1\, p_2\, \pi_3^+ \qquad (2a)$$

respectively; the subscript "S" denotes a spectator, either in the beam deuteron "B" or the target deuteron "T".

1. Scanning and Measurement

a. n-n events. In reaction (1a) the target spectator proton is

not seen in the bubble chamber in 70% of the interactions because its momentum is less than 90 MeV/c. Therefore, we scanned for events with three outgoing charged particles, since the proton in the target deuteron is then clearly a spectator. (Here we did not worry about the four-prong events because of the difficulty of distinguishing p_S^T from p_1.) In scanning we used only two views (V2 and V3) unless there was an ambiguous event, in which case we referred to the other two views.

The scanned events were then measured in three views (V1, V2 and V3) on a "Franckenstein", which is a motor-driven digitized projector with a servo-mechanism which centers automatically on the track. The measurement consists of determining the location of a series of points along a track with respect to fiducial marks.

All told, 2870 three-prong events were measured and constrained to the hypothesis:

$$d\ n \rightarrow p\ p\ n\ \pi^- \qquad (1b)$$

assuming that the target neutron was at rest in the laboratory system, with a beam deuteron momentum of 3.64 ± .01 BeV/c. The (1b) events include not only n-n events, but also some p n reactions of the type:

$$d\ d \rightarrow n_S^B\ p_S^T\ p\ p\ \pi^-.$$

The subtraction of p n events from the sample is described below.

The deuteron beam momentum was obtained by measuring the curvature of 202 beam tracks of lengths greater than 30 cm. Figure 3 shows the distribution in $1/p_D$, which is more symmetric than the distribution in p, itself. From this we estimated the beam momentum of 3.641 ± .006 BeV/c, which is equivalent to the curvature of (13.72 ± .02) x 10^{-4} cm^{-1}. The width of the distribution indicates an average error in the sagitta in the chamber of 40 μ. This agrees with the known setting error. As

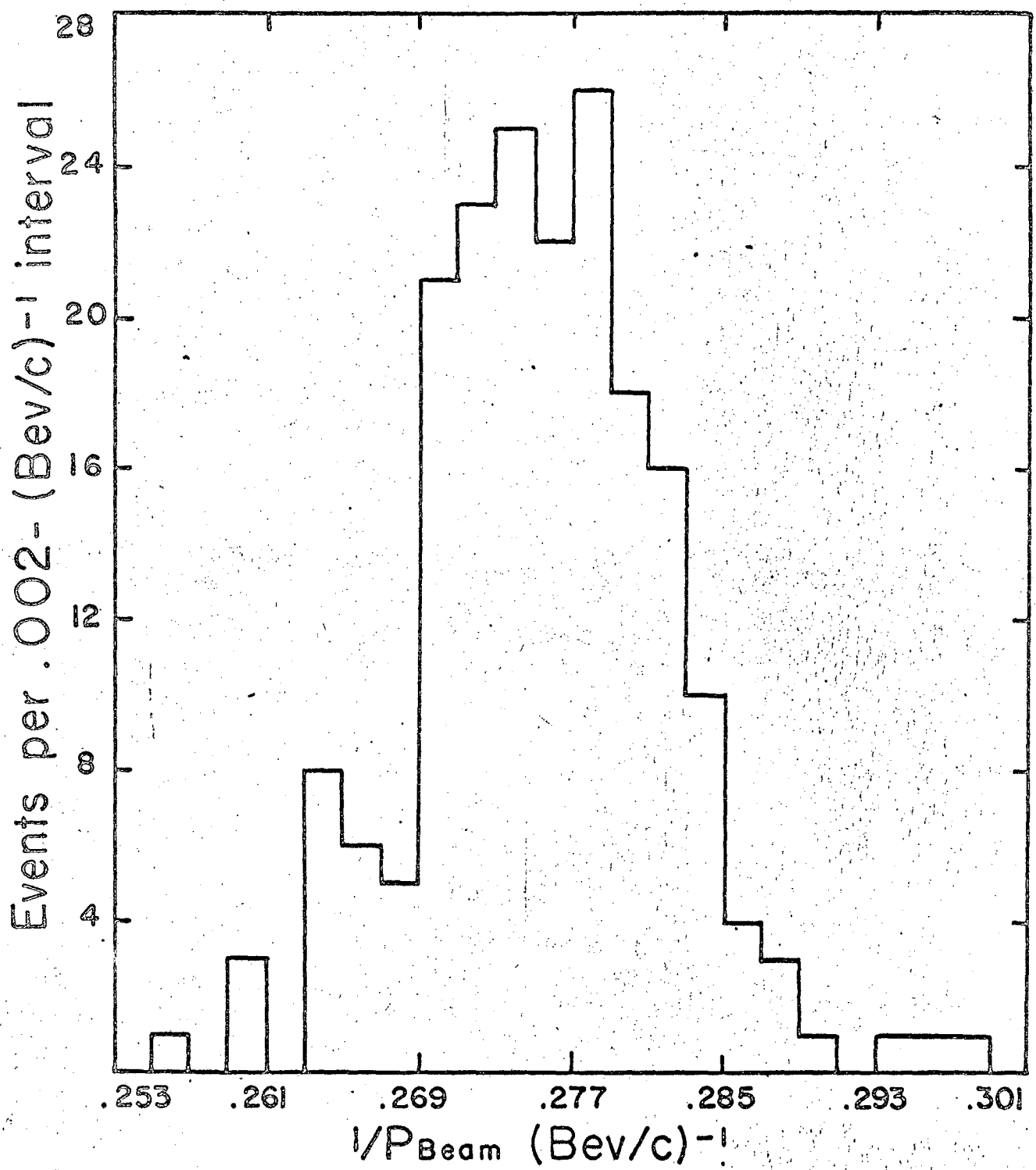
Events per .002-(Bev/c)⁻¹ interval
28
24
20
16
12
8
4
.253
.261
.269
.277
.285
.293
.301
1/P Beam (Bev/c)⁻¹

Fig. 3

a check, we also obtained the beam momentum from the computed missing mass, M_o, given by $M_o^2 = E_N^2 - P_N^2$, where "N" stands for the neutral particle. This value is systematically shifted from the true missing mass, M_o^*, because of the correlation in the errors on E_N and P_N. The correction for this is made with the formula,[15]

$$M_o^{*2} = M_o^2 + \sum_{i=\pi,N} \left(\frac{\Delta P_i}{\gamma_i}\right)^2 \left(1 - \frac{E_\pi + E_N}{E_i}\right).$$

Using this formula, we obtain $M_o^* = .938 \pm .004$ BeV (neutron mass in reaction (1b)) with a beam momentum of 3.64 BeV/c. In this experiment the relation between the change in missing mass, ΔM_o, and the change in beam momentum, ΔP_D, is given by $\Delta M_o = .3 \Delta P_D$ (i.e., a 1% change in beam momentum causes a shift of 12 MeV in the missing mass). Therefore, the observed value of M_o^* indicates a beam momentum of $3.64 \pm .01$ BeV/c. Figure 4 shows the distribution in the corrected missing mass squared.

b. <u>p-p events.</u> The p-p ($p\ p \rightarrow n\ p\ \pi^+$) events in reaction (2a), $d\ d \rightarrow n_S^T\ n_S^B\ n_1\ p_2\ \pi_3^+$, were found by scanning for events with two emergent positively charged particles (p and π^+). Since both tracks are of the same charge, there is a problem of distinguishing π^+ from proton. However, in reaction (1a) the maximum π^--meson momentum is 900 MeV/c and its mean value 350 MeV/c, and the π^+-meson in (2a) should have the similar distribution. Therefore, the π^+ is readily identified by momentum and bubble density. Unlike reaction (1a) which contains only one neutral particle, reaction (2a) has three neutral particles. Consequently, it is not possible to employ such constraining equation as $d\ p \rightarrow n\ n\ p\ \pi^+$, which is charge symmetric to (1b), $d\ n \rightarrow p\ p\ n\ \pi^-$. Instead, we had to constrain the two-prong events to the hypothesis,

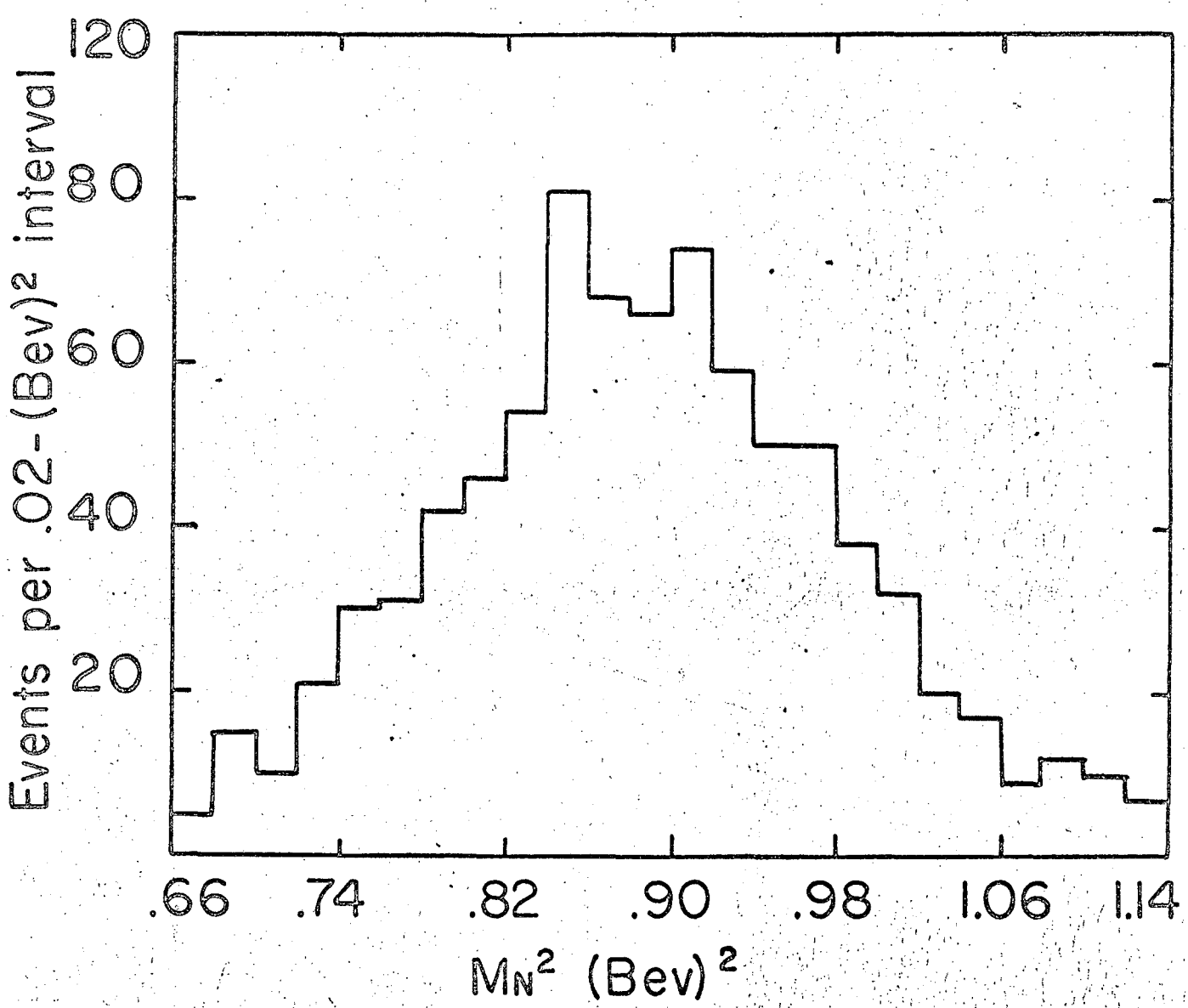
Events per .02-(Bev)² interval
120
80
60
40
20
.66
.74
.82
.90
.98
1.06
1.14
MN² (Bev)²

Fig. 4

$p\ p \rightarrow n\ p\ \pi^+$, the reaction (2). Altogether, 1687 events were measured and were constrained to this hypothesis with a beam proton momentum of 1.82 ± 0.09 BeV/c and the target proton assumed to be at rest. Here the direct measurement of the beam proton momentum is not possible because the beam proton is still part of the deuteron with a (known) momentum distribution. As a result, the mean beam proton momentum is just one-half of the beam deuteron momentum, 3.64 BeV/c with a momentum spread which is simply obtained by transforming the Hulthén deuteron wave function in the beam deuteron rest frame to the laboratory system (Fig. 5). This distribution is approximated fairly closely by a Gaussian with a standard deviation σ = 0.09 BeV/c.

2. Data Analysis

The measured events were processed on the IBM 7094 computer using the FOG-CLOUDY-FAIR data reduction system.[16] FOG reconstructs the spatial position of each track by finding the dip angle and the azimuthal angle. Here the momentum of the particle is also computed. It also applies a series of checks on the measurement input for errors that might have been made during the measurement. CLOUDY calculates the errors on angles and momenta. It applies kinematic constraints, compatible with energy and momentum conservation at each vertex, by the method of least squares. To do that, it minimizes the quantity M defined by

$$M(\chi_i, \alpha_\lambda) = \sum_{i=1} \frac{(\chi_i - \chi_i^M)^2}{\Delta_i^2} - 2 \sum_{\lambda=1}^{4} \alpha_\lambda F_\lambda (\chi_i),$$

where χ_i^M is the measured value of χ_i, Δ_i is the error on χ_i, α_λ are the Lagrangian multipliers, and F_λ are the four constraining equations for longitudinal momentum, transverse momentum, coplanarity and total energy

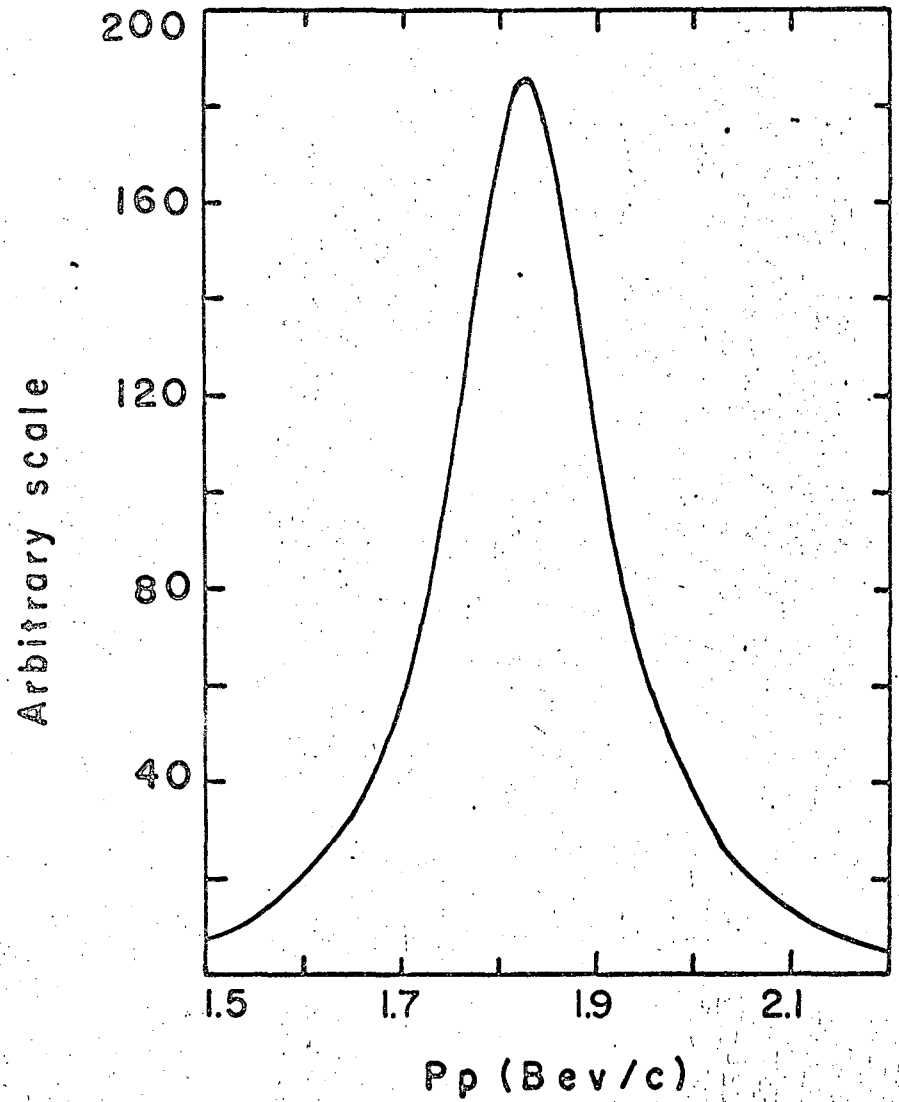

Fig. 5

at a vertex. The minimum value of M occurs when all the F's are zero, whereby M becomes a χ^2 test for the goodness of fit for each assumption. FAIR organizes the results of the computations and presents the output in various forms.

The effect of ignoring the target motion in constraining reactions (1b) and (2) is to broaden the χ^2 distributions (Fig. 6), relative to a χ^2 distribution for a genuine one-degree-of-freedom event. In a one-constraint fit the χ^2 value is approximately $\left[(MM - MN) / \Delta MM \right]^2$, where MM is the calculated missing mass, MN is the true mass of the outgoing neutral particle, and Δ MM is the experimental error in missing mass. Neglect of the target momentum P_T shifts the missing mass downward by an amount $(T_T \cdot T_n - \underset{\sim}{P}_T \cdot \underset{\sim}{P}_n) / MM$, where T_T is the kinetic energy of the target particle and P_n and T_n are the momentum and kinetic energy of the outgoing neutral particle. There is a correlation between large χ^2 values and high momenta of the outgoing neutral particle. For this reason it was necessary to accept all nn and pp events with $\chi^2 \leq 10$.

The χ^2 criterion was used to identify the events only; we did not use the constrained values of the particle momenta because of the uncertainty in the target momentum. In calculating the $(\pi^+ p)$ and $(\pi^- n)$ invariant masses we used the measured values of the particle momenta, and the neutron momentum was inferred from momentum conservation in reaction (1b) with the target neutron assumed to be at rest. The neutron momentum is then uncertain by P_T, the target momentum, in addition to the usual measurement errors. In consequence, the calculated $(\pi^- n)$ invariant mass, $\omega_{\pi^- n}$, is reduced from its true value by $\Delta Q = \left[(E_\pi / E_n) \cdot (\underset{\sim}{P}_n \cdot \underset{\sim}{P}_T) - (\underset{\sim}{P}_\pi \cdot \underset{\sim}{P}_T) \right] / \omega_{\pi^- n}$. A Monte Carlo calculation shows that

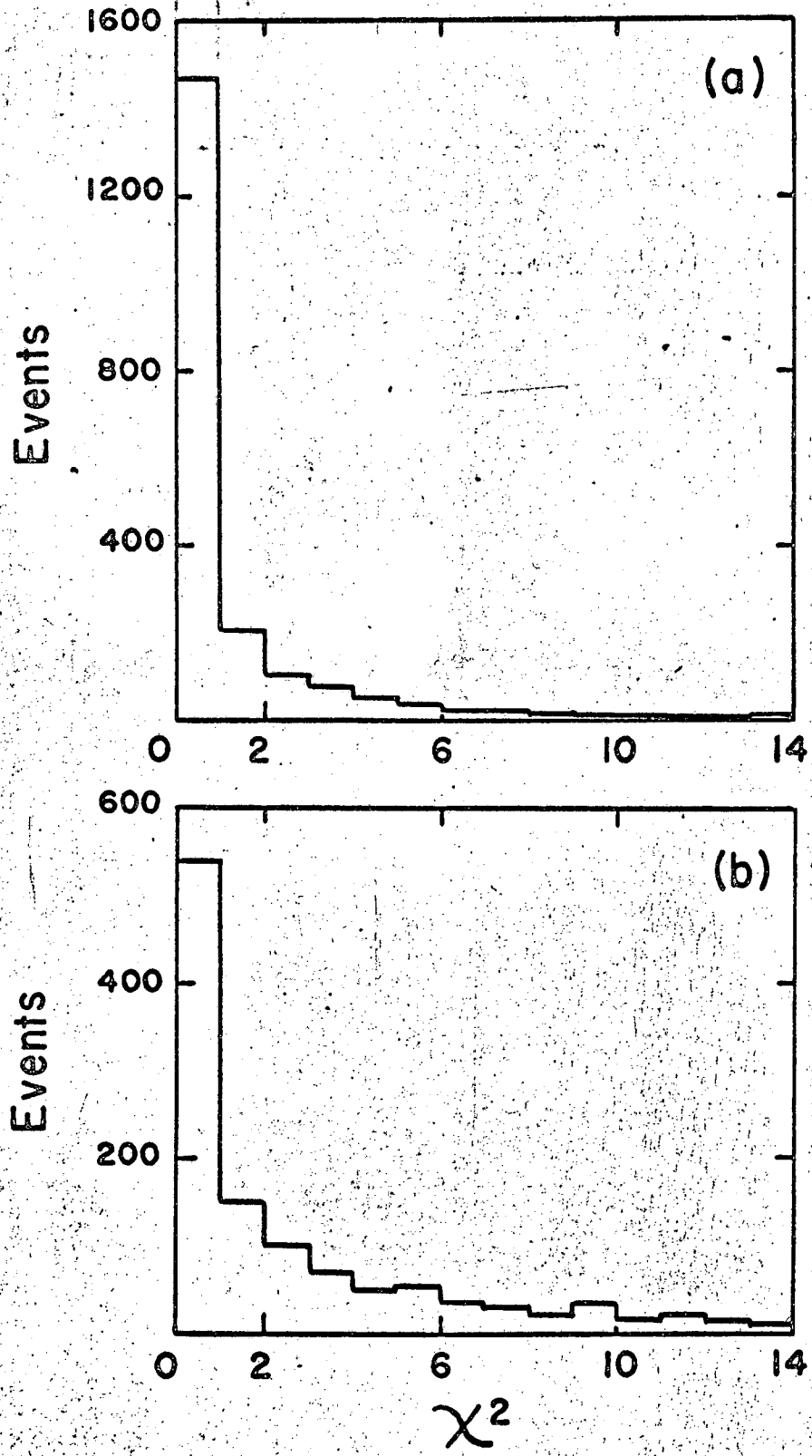
(a)
1600
1200
800
400
Events
0
2
6
10
14
(b)
600
400
200
Events
0
2
6
10
14
χ^2

Fig. 6

ΔQ has a distribution with mean of -0.2 MeV, and root-mean-square deviation 6 MeV; its effect on the mass and width of the $(\pi^- n)$ distribution can therefore be ignored. Two additional criteria were applied to enforce a correspondence between the nn and pp events.

(a) There may be a scanning bias against pp events with a short proton track. Hence we eliminated pp events with $P_p < 150$ MeV/c, and nn events with $P_n < 150$ MeV/c.

(b) The uncertainty in ω_{23}, due to measurement errors, is greater for $(\pi^- n)$ than for $(\pi^+ p)$. The average experimental error in ω_{23} is 30 MeV for $(\pi^- n)$ and 20 MeV for $(\pi^+ p)$ (Fig. 7). We eliminated all events with an error exceeding 20 MeV. (No correlation was observed between ω_{23} and its error.) Then the experimental error is the same in both reactions, and is small compared with the resonance width (Γ_o = 120 MeV for N^{*++}). This condition is important because the value of the resonant mass inferred from the invariant-mass distribution is not independent of the width of the distribution.

C. Subtraction of Background from the Invariant-Mass Plots

Before the resonance parameters are inferred from the invariant-mass plots, certain background events must be subtracted. These are:

(a) pn reactions which are mixed in with the nn events, and

(b) nn and pp reactions which do not proceed via N^{*-} and N^{*++} production, respectively.

(a) For the nn events in reaction (1b) the beam proton is a spectator; in the pn event the beam neutron is a spectator. A beam spectator is identified by having a momentum of less than 120 MeV/c in

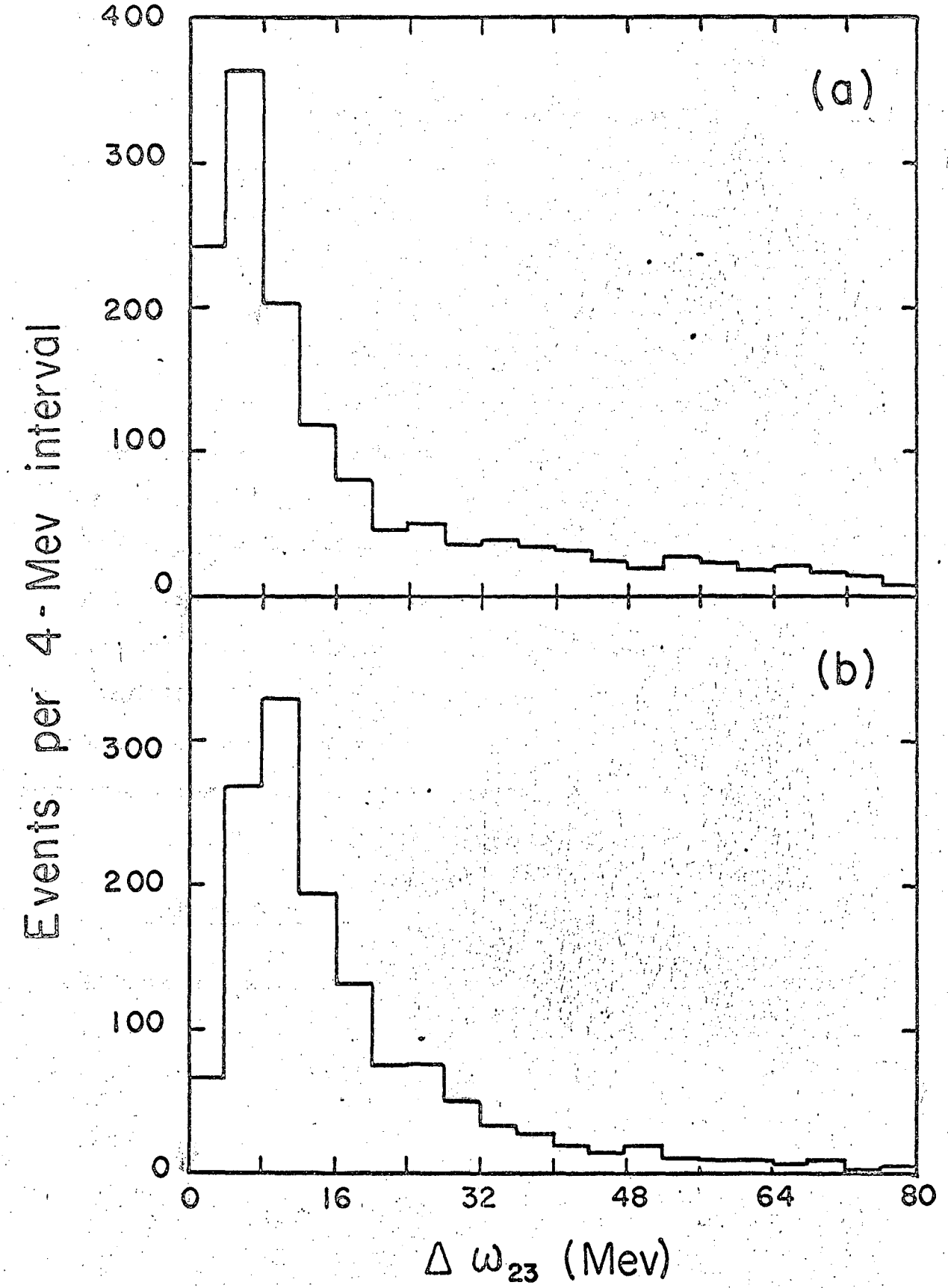
400
300
200
100
0
(a)
(b)
300
200
100
0
Events per 4-Mev interval
0
16
32
48
64
80
Δ ω23 (Mev)

Fig. 7

the rest system of the beam deuteron. The transverse momentum distribution of such nucleons is shown in Fig. 8; it follows closely the Hulthén form of the deuteron wave function, giving evidence for the validity of the impulse approximation. Appendix A discusses the structure of the deuteron and the impulse approximation. In a total of 1091 dn interactions, 133 had a beam spectator neutron and did not have a beam spectator proton. (In a strongly peripheral interaction, the interacting nucleon is sometimes indistinguishable from a spectator.) The $(\pi^- n)$ effective mass distribution for these 133 events is shown in Fig. 9. They are clearly $pn \rightarrow pp\pi^-$ reactions, as there is no evidence of N^{*-} production. According to the measured nucleon-nucleon cross-sections in this energy region the ratio of nn to pn interactions is 5.2.[17] The expected number of pn events is then 176; the discrepancy is due to the experimental error in the neutron momentum which can shift it outside the limits for a high-energy spectator—$1.4 < \underline{P} < 2.3$ BeV/c, $0 \text{ deg} < \Theta < 5$ deg—where $\underline{P}$ is the neutron momentum and Θ is the angle it makes with the beam. The distribution in Fig. 9 was normalized to a total of 176 events and subtracted from the $(\pi^- n)$ invariant mass distribution (1091 events).

(b) It is known that reactions (1) and (2) are dominated by one-pion exchange (OPE) in this energy region.[18,19] (The applicability of OPE model in this experiment is shown in section IV.) If the reaction mechanism is purely one-pion exchange, and if N^* production is the rule, it is possible to show from simple isotopic spin considerations that charged pion exchange predominates over neutral pion exchange in the proportions 9:1. Experimental observations are in agreement with this prediction.[18,19] Figure 10 shows the comparison of the distribution of

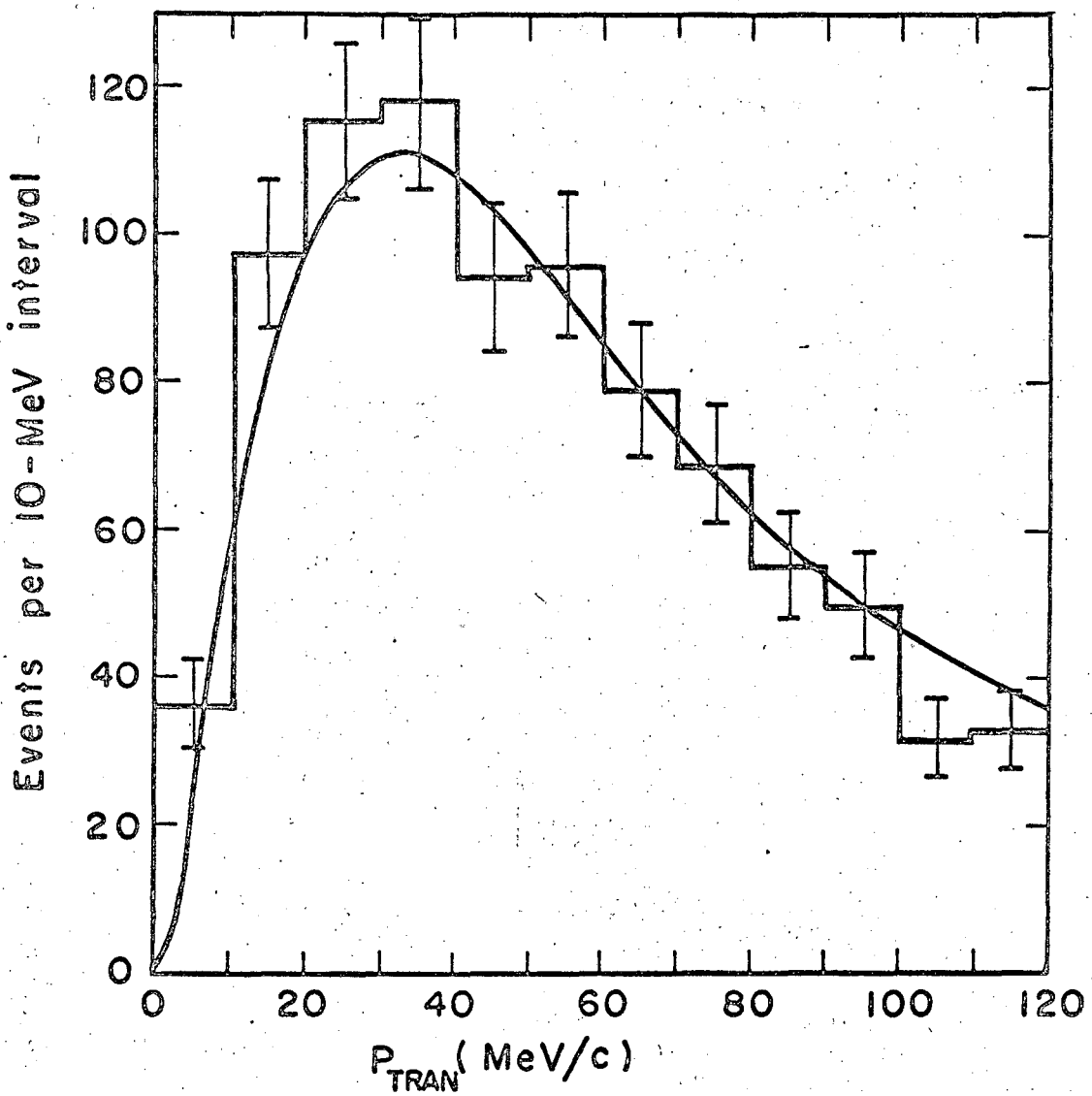
Events per 10-MeV interval
0
20
40
60
80
100
120
0
20
40
60
80
100
120
P_{TRAN} (MeV/c)

Fig. 8

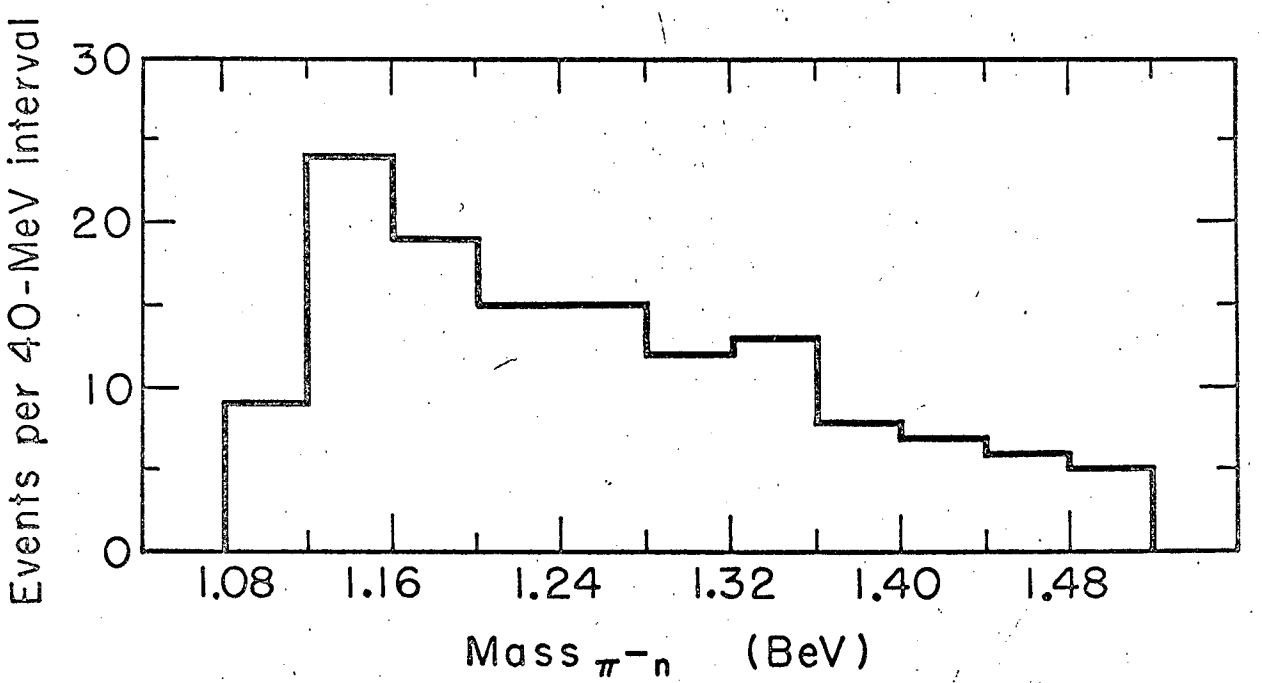

MUB-6252

Fig. 9

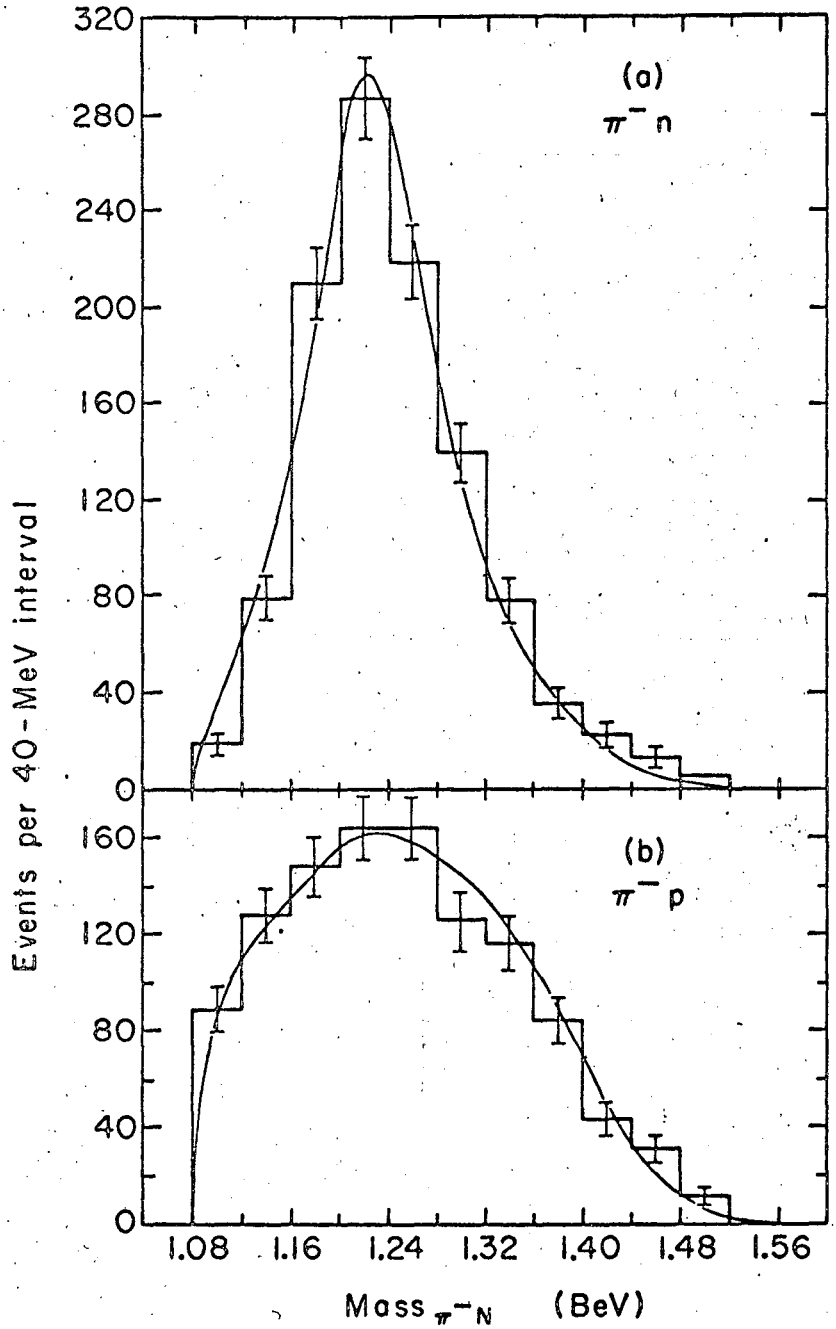
(a)
$\pi^- n$
(b)
$\pi^- p$
Events per 40-MeV interval
Mass $_{\pi^- N}$ (BeV)
320
280
240
200
160
120
80
40
0
160
120
80
40
0
1.08
1.16
1.24
1.32
1.40
1.48
1.56
MUB-6629

Fig. 10

invariant masses, ω_{π^-n} and ω_{π^-p} in reaction (1), with the theoretical curves, which are the predictions of the Breit-Wigner formula, multiplied by the three-body phase space and then weighted according to the ratio of 9:1 for the N^{*-} (π^-n) and N^{*o} (π^-p) productions. They agree quite well. Under these conditions the reflection of N^{*o} and N^{*+} in reactions (1) and (2) is closely approximated by the (π^-p) invariant-mass distribution in reaction (1) (Fig. 10(b)). This distribution, normalized to 10% of the areas of the invariant mass plots ω_{23}, has been subtracted from both these plots. By making the correction in this manner, the range of interaction energies is properly taken into account, and we avoid the problem of calculating the reflection.

The corrected effective mass distributions are shown in Fig. 11. They contain a total of 695 nn and 558 pp events in the interval 1140 to 1320 MeV. These numbers do not reflect the relative cross-sections, because not all the photographs used for the nn interactions were scanned for pp interactions.

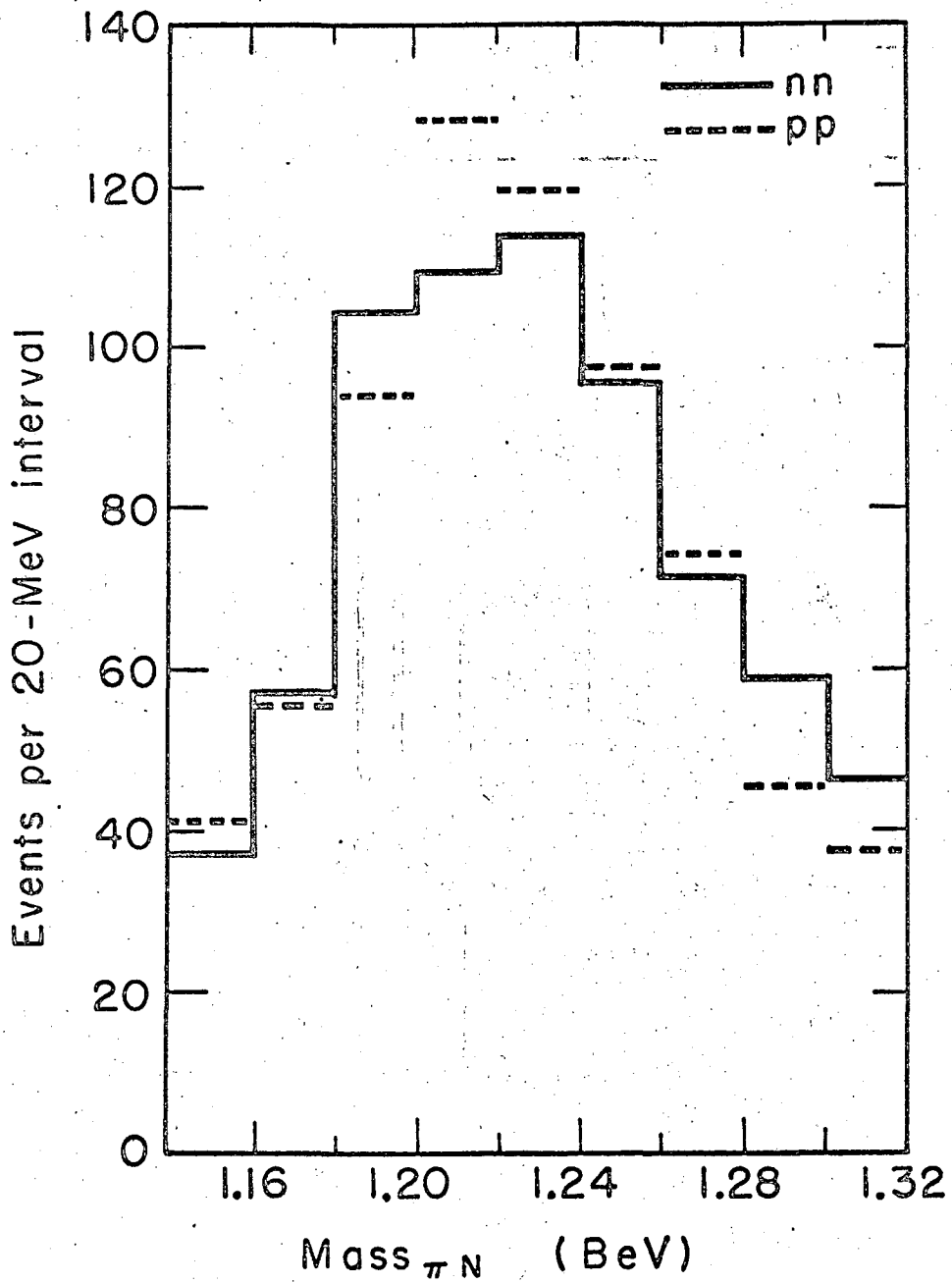

MUB-6254

Fig. 11

III. POSSIBLE SOURCES OF ERROR

Because the mass of N^{*-} in reaction (1) n n → p n π^- is determined using the momentum of the neutron in the final state which was inferred from momentum conservation in reaction (1b) d n → p_S^B p n π^- while the mass of N^{*++} in reaction (2) p p → n p π^+ is determined with the momenta of two charged particles, p and π^+, which were directly measured, systematic errors in the beam momentum or the magnetic field (or both) can simulate an additional mass difference. This danger is avoided by using the value of the beam momentum obtained by curvature measurement on beam tracks in the bubble chamber. If the magnetic field value is incorrect (say, by 1%), the pion and proton momentum are overestimated by 1%, but the neutron momentum is similarly affected, since it is calcualted as $\underset{\sim}{P}_n = \underset{\sim}{P}_d - \Sigma \underset{\sim}{P}_{charged}$. Thus, there is no spurious mass difference induced by an incorrect value for the magnetic field, provided the beam momentum is estimated by use of the same value for the magnetic field.

A systematic curvature in the chamber would change the beam momentum and shift the (π^-n) invariant-mass distribution. The maximum systematic curvature in the chamber has been estimated at 0.1 x 10^{-4} cm^{-1} (Fig. 12), equivalent to 1% of the beam momentum.[14] A 1% change in beam momentum causes an average shift of 1 MeV in the effective mass. In fact, there is strong evidence that the systematic curvature in the chamber is considerably less than the maximum value quoted.[14]

In reaction (1) target neutrons with momenta greater than 90 MeV/c are excluded. Hence, the range of C. M. energies in reaction (1) is restricted compared with reaction (2) (Fig. 13). However, the requirement of a fit of reaction (2) has the effect of excluding high Fermi

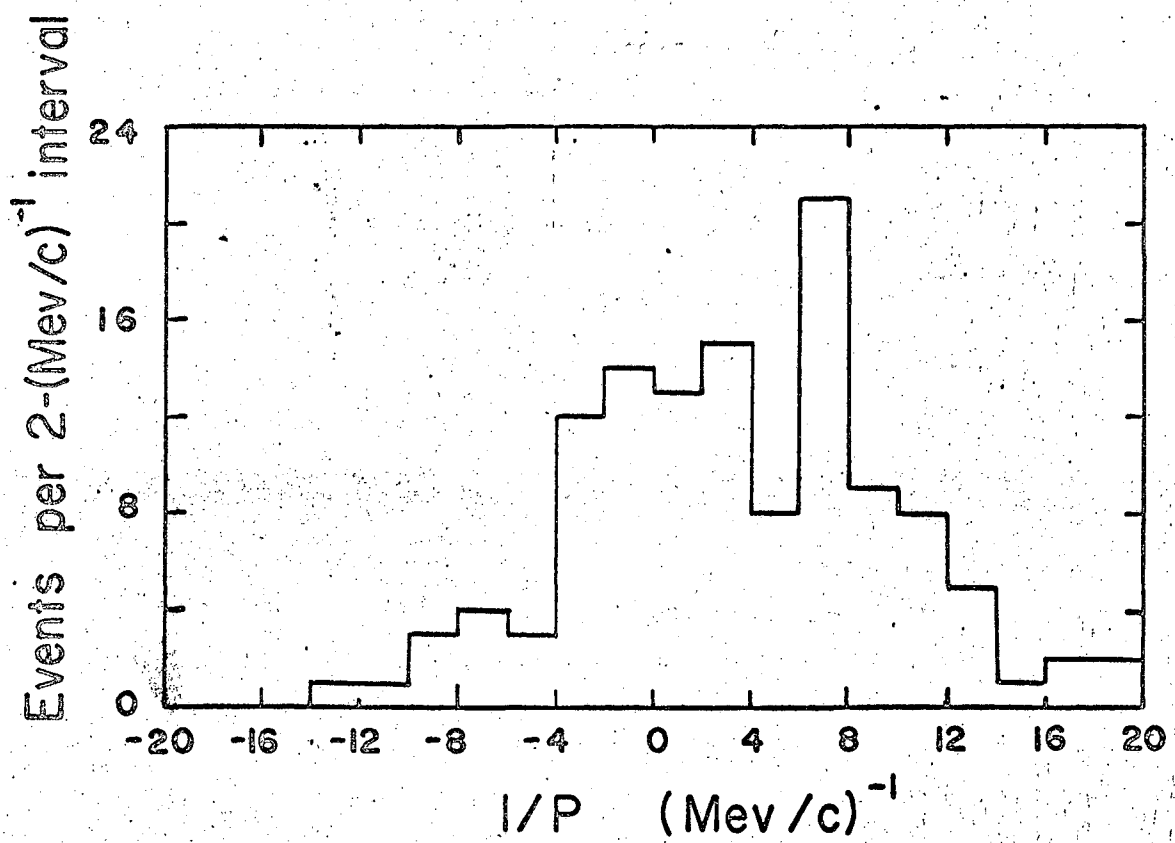
Events per 2-(Mev/c)$^{-1}$ interval
24
16
8
0
-20
-16
-12
-8
-4
0
4
8
12
16
20
1/P (Mev/c)$^{-1}$

Fig. 12

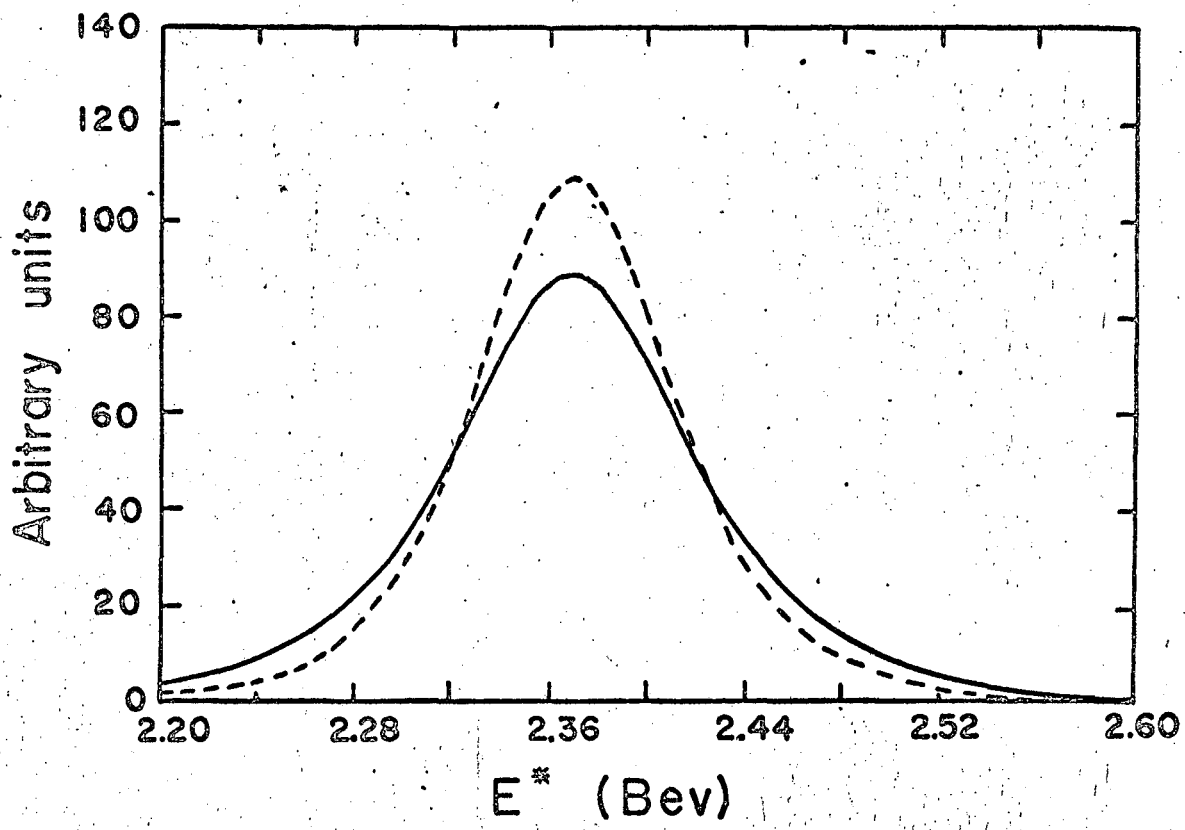
140
120
100
80
60
40
20
0
Arbitrary units
2.20
2.28
2.36
2.44
2.52
2.60
E* (Bev)

Fig. 13

momenta. As a check on the equality of the range of interaction energies for the two reactions, the pion and nucleon momentum distributions are compared in Figs. 14(a) and 14(b). The coincidence of the momentum spectra leads us to believe that there is no bias here.

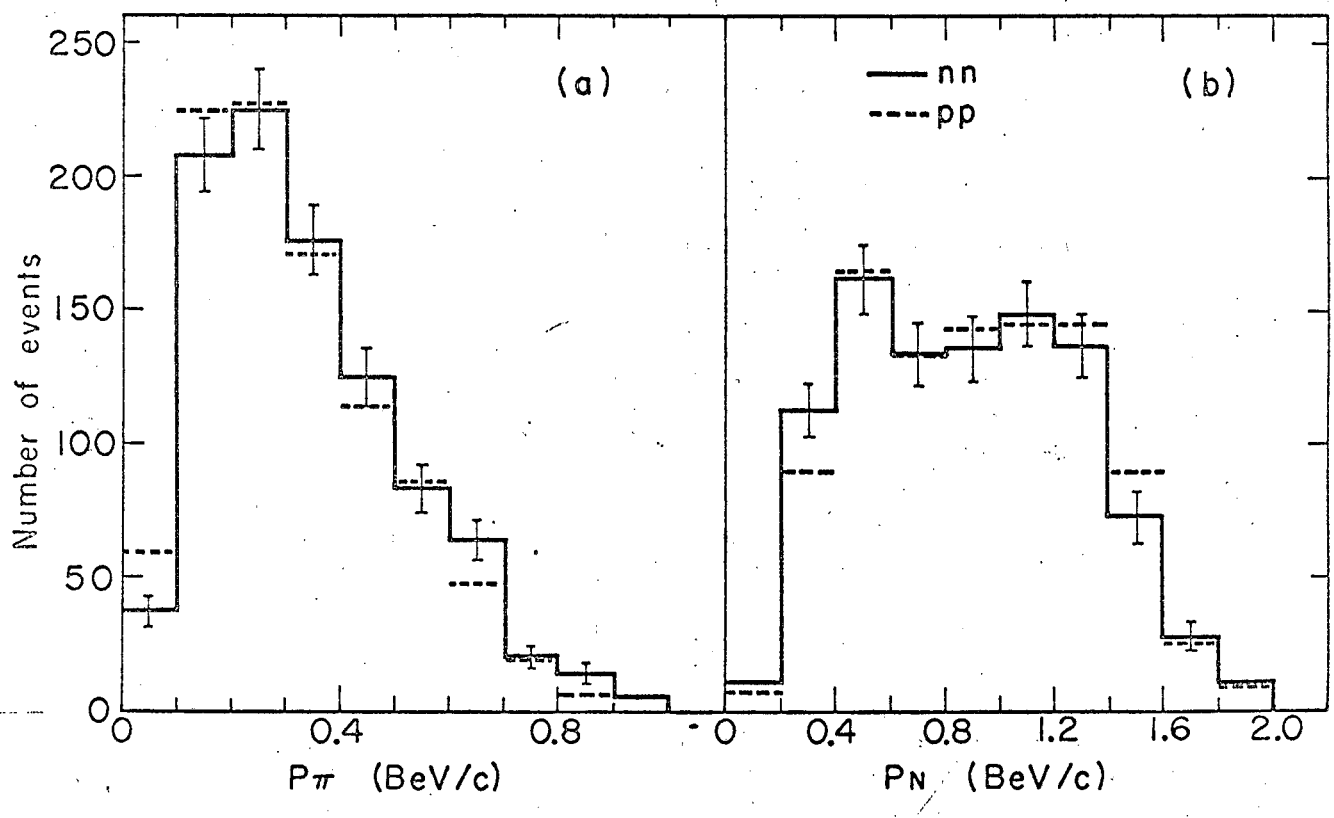
250
200
150
100
50
0
Number of events
(a)
(b)
nn
pp
0
0.4
0.8
0
0.4
0.8
1.2
1.6
2.0
Pπ (BeV/c)
PN (BeV/c)
MUB-6255

Fig. 14

IV. ONE-PION-EXCHANGE MODEL

Although an exact quantitative description of the production mechanism is not available here, we know that the OPE (one-pion-exchange) model has been quite successful in describing the experimental data on p-p reactions ($p\ p \rightarrow n\ p\ \pi^+$) over the range of proton laboratory energies from 1 to 3 BeV.[20] If the OPE dominates both n-n ($n\ n \rightarrow p\ n\ \pi^-$) and p-p reactions in this experiment, the N^{*-}-N^{*++} mass difference can be estimated more accurately with the OPE formula than with the formula obtained with constant matrix element.

If the OPE theory works for $p\ p \rightarrow n\ p\ \pi^+$, the principle of charge symmetry implies that it should also work for the charge symmetric reaction, $n\ n \rightarrow p\ n\ \pi^-$. However, this principle has not been accurately tested in the BeV energy region. Therefore, it was necessary for us to verify the applicability of the OPE model for the n-n reaction in this experiment.

Figure 15 shows the center-of-mass angular distributions for the outgoing nucleons in the reaction, $n\ n \rightarrow p\ n\ \pi^-$. These are sharply peaked forward and backward indicating that the reaction is predominantly peripheral. This peaking is expected if the reaction goes mainly through the exchange of a virtual pion between the two nucleons, with scattering of the virtual pion by one of the nucleons. There are then four diagrams (Fig. 16) to describe this reaction. Chew and Low have shown that the OPE reaction occurs primarily at low values of Δ^2, which is the square of the four-momentum of the virtual pion. By employing the physical principle of the existence of poles in the S-matrix corresponding to the exchange of single particle in the intermediate state, they proposed the so-called pole-approximation cross-section. This cross-

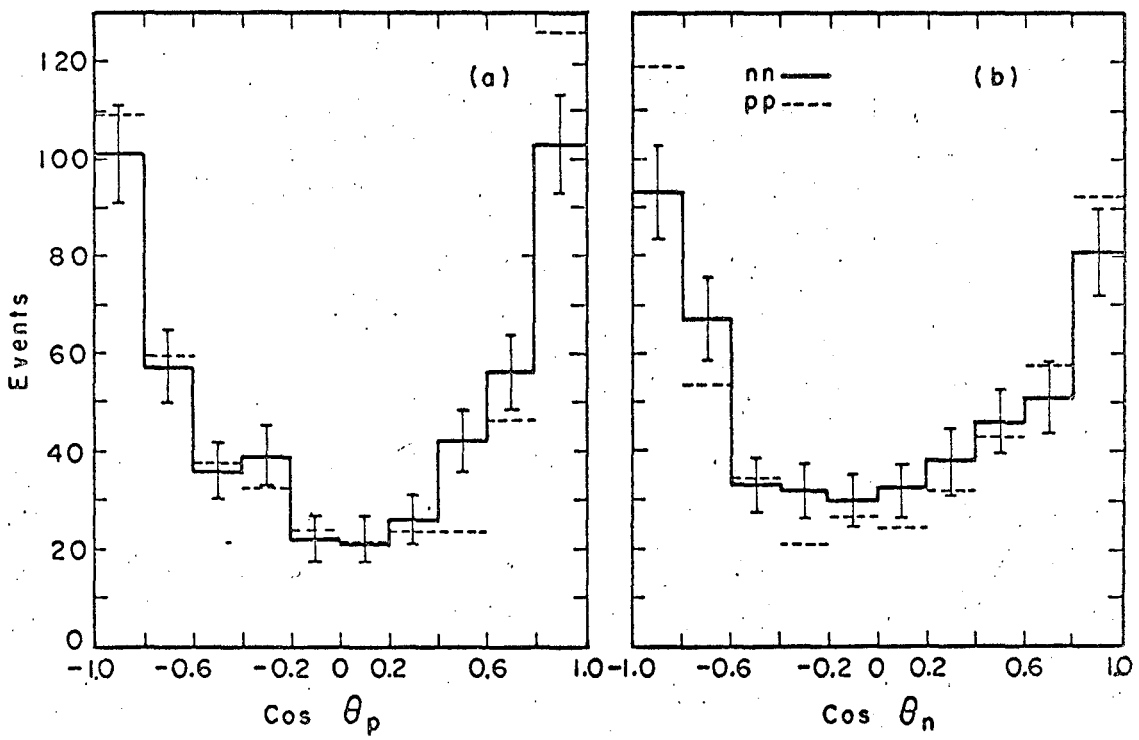
(a)
(b)
nn
pp
Events
120
100
80
60
40
20
0
-1.0
-0.6
-0.2
0
0.2
0.6
1.0
Cos θ_p
Cos θ_n
MUB-3353

Fig. 15

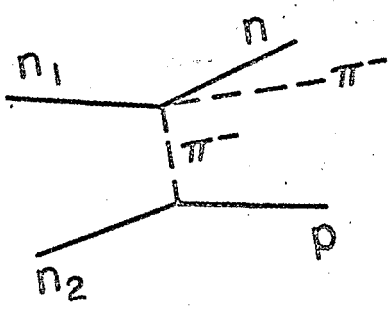

(a)

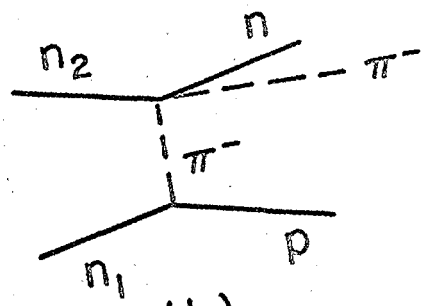

(b)

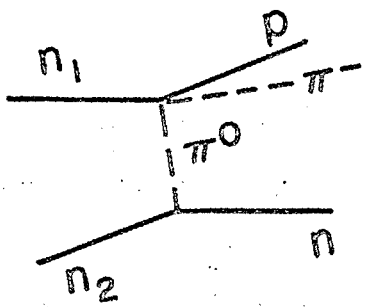

(c)

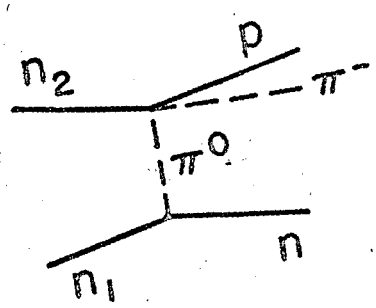

(d)

MUB-7412

Fig. 16

section is proportional to $\Delta^2/(\Delta^2 + M_\pi^2)^2$ in the non-physical limit, as $\Delta^2 \to -m_\pi^2$. Subsequently, Ferrari and Selleri, assuming that the Chew-Low formula is valid even in the physical region, deduced an OPE formula.[20] Introducing a single empirical form factor to this formula, they succeeded in fitting the p-p ($p\ p \to n\ p\ \pi^+$) data at 970 MeV, 2.85 BeV and 3 BeV.[20]

For the n-n reaction ($n\ n \to p\ n\ \pi^-$), we compare (in Fig. 17) the distribution of the laboratory kinetic energy of the proton with the prediction of the OPE formula of Ferrari and Selleri, weighted according to the known distribution of reaction energies (Fig. 18). The agreement is quite good, indicating the dominance of OPE in this reaction. The sharp peak at low energy corresponds to the proton recoil following the pion emission by the target neutron and the broader peak at high energy is due to pion emission by the beam neutron. The broadening is a consequence of the transformation from the beam neutron rest frame to the laboratory system.

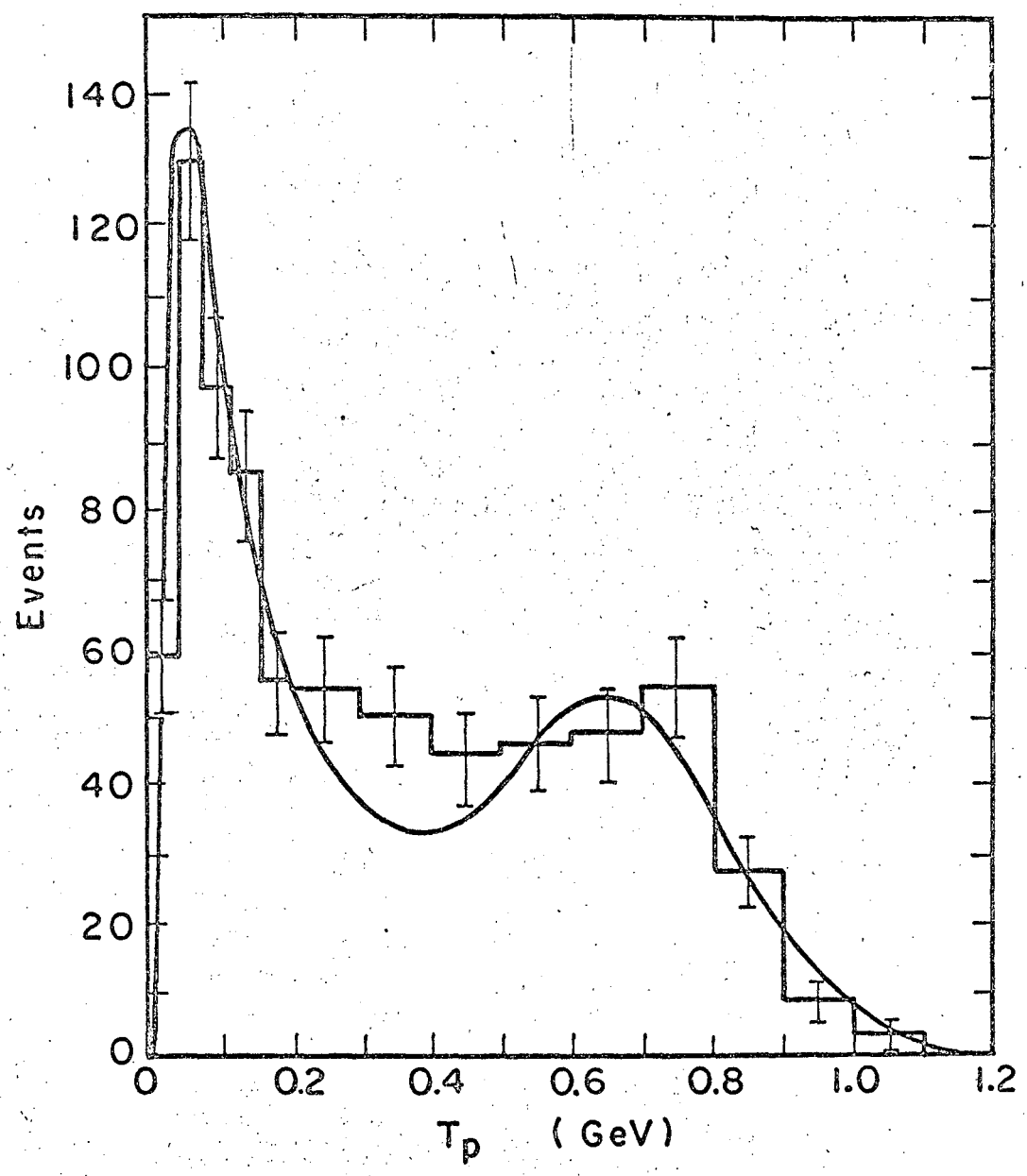

Fig. 17

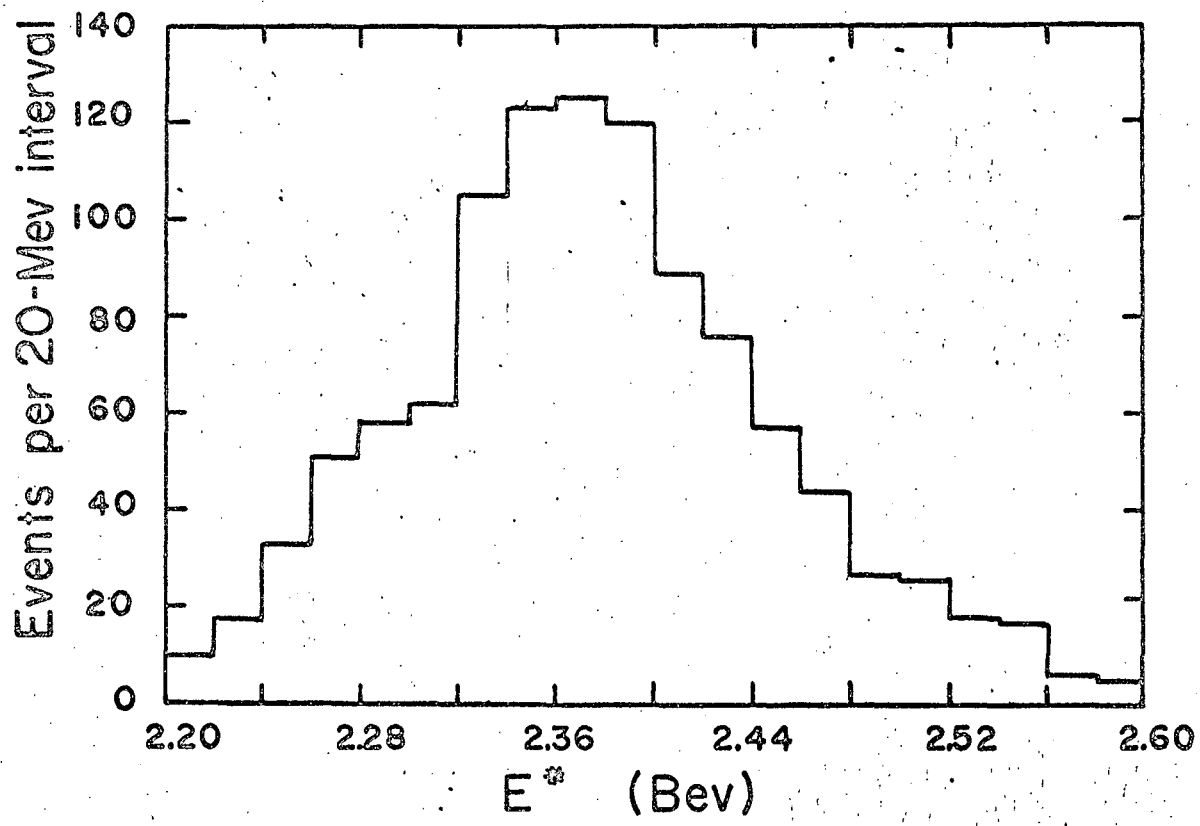
Events per 20-Mev interval
0
20
40
60
80
100
120
140
2.20
2.28
2.36
2.44
2.52
2.60
E* (Bev)

Fig. 18

IV. Determination of the Resonance Parameters

The differential cross section for Reaction (1) is

$$d\sigma \propto |A|^2 \, \delta^4 (P_f - P_i) \, \frac{d^3 p_1 \, d^3 p_2 \, d^3 p_3}{E_1 \, E_2 \, E_3} \, ,$$

where A is the reaction amplitude. If A is known, one can calculate the $(\pi^- n)$ invariant-mass distribution $\frac{d\sigma}{d\omega} (\omega, \omega_0, \Gamma_0)$. The most probable values of ω_0 and Γ_0 are those which minimize χ^2 when the experimental distribution in ω is fitted with $\frac{d\sigma}{d\omega}$. Because the production mechanism is not completely understood, no absolute determination of ω_0 and Γ_0 is attempted in this experiment.

Since the two resonances are produced in charge-symmetric reactions, we assume that the mass difference can be evaluated by use of an approximate expression for the amplitude. The validity of the approximation is tested by comparing the calculated N^{*++} parameters with the values measured directly in $\pi^+ p$ elastic scattering.

Analyses of Reactions (1) and (2) in this energy region[18,19] strongly indicate that: (a) the reactions go predominantly by one-pion exchange (OPE), and (b) the virtual π-nucleon scattering is dominated by the N^* resonant amplitude. We use these results to obtain an approximate expression for $\frac{d\sigma}{d\omega}$.

The amplitude for the reaction is

$$A = A_a - A_b - A_c + A_d,$$

where the subscripts refer to the corresponding OPE diagrams in Fig. 16. The interference terms $A_a A_d^*$ and $A_b A_c^*$ vanish because of the pseudoscalar nature of the pion, and it has been shown that the terms $A_a A_c^*$ and $A_b A_d^*$ are negligible.[20] Then

$$|A|^2 = |A_a|^2 + |A_b|^2 - 2 \text{ Re } A_a A_b^* + |A_c|^2 + |A_d|^2 - 2 \text{ Re } A_c A_d^*.$$

It is convenient to split $d\sigma$ into the sum of six terms, corresponding to these six terms:

$$d\sigma = d\sigma_a + d\sigma_b + d\sigma_{ab} + d\sigma_c + d\sigma_d + d\sigma_{cd}.$$

In the pole approximation (exchanged pion on the mass shell) the partial cross section $\frac{d\sigma_a}{d\omega}$ is[21]

$$\frac{d\sigma_a}{d\omega} \propto \int_{\Delta^2_{MIN}}^{\Delta^2_{MAX}} k\,\omega^2\,\sigma(\omega)\,\frac{\Delta^2}{(\Delta^2 + m_\pi^2)^2}\,d\Delta^2 = \sigma(\omega)\,f(\omega), \qquad (3)$$

where ω is the $(\pi^- n)$ effective mass, k is the π^- momentum in the $(\pi^- n)$ rest frame, Δ^2 is the square of the four-momentum of the exchanged pion, and $\sigma(\omega)$ is the cross section at the four-particle vertex. It is clear that $\frac{d\sigma_a}{d\omega} = \frac{d\sigma_b}{d\omega}$ and $\frac{d\sigma_c}{d\omega} = \frac{d\sigma_d}{d\omega}$. We evaluated $\frac{d\sigma_{ab}}{d\omega}$, using the expression for $d\sigma_{ab}$ derived by Selleri in the pole approximation.[20] We found that $\frac{d\sigma_{ab}}{d\omega} = \sigma(\omega)\,f_I(\omega) \approx (0.6)\,\sigma(\omega)\,f(\omega)$. Since $f_I(\omega)$ is almost identical in form with $f(\omega)$, we made the approximation

$$\frac{d\sigma}{d\omega} \propto \frac{d\sigma_a}{d\omega} + \frac{d\sigma_c}{d\omega}.$$

As discussed in Section IIC, N^{*-} production ($d\sigma a$) predominates over N^{*o} production ($d\sigma c$) in the proportions 9:1. Approximating the shape of the $(\pi^- n)$ effective mass distribution for the $nn \rightarrow nN^{*o}$ events by the $(\pi^- p)$ effective mass distribution in Reaction (1), we were able to subtract out the events corresponding to the N^{*o} production. A similar procedure was used to eliminate the reflection of N^{*+} in the $(\pi^+ p)$ invariant-mass plot. The resulting distributions in Fig. 11 correspond to pure N^{*-} and N^{*++} productions and are described by $\frac{d\sigma_a}{d\omega}$.

The distributions in Fig. 11 were fitted with Eq. (3), modified by the off-the-mass-shell correction term[22]

$$\left[\frac{(\omega + m_2)^2 + \Delta^2}{(\omega + m_2)^2 - m_\pi^2}\right]^2 \quad \left[\frac{(\omega - m_2)^2 + \Delta^2}{(\omega - m_2)^2 - m_\pi^2}\right] .$$

This factor is discussed in Appendix C. The upper limit for Δ^2 was set at 0.8 $(\text{BeV}/c)^2$, according to the observed Δ^2 distribution in the nn reactions. In fact, the result is insensitive to a 50% variation in Δ^2_{MAX}. We use a single resonant p-wave amplitude for the π-nucleon cross section σ :

$$\sigma(\omega) \quad \frac{\omega_0^2 \Gamma^2(\omega)}{(\omega_0^2 - \omega^2)^2 + \omega_0^2 \Gamma^2(\omega)} ,$$

with $\Gamma = \Gamma_0 (q/q_0)^3 \rho(\omega)/\rho(\omega_0)$,

where $\rho(\omega) = (a m_\pi^2 + q^2)^{-1}$ and $a = 1.3$ for m_π and q in MeV units;[22] q is the momentum of the decay products in the N^* rest frame. The values of ω_0 and Γ_0 which minimize χ^2 are shown in Table II. (It is reassuring that the N^{*++} parameters are in good agreement with the values measured in elastic $\pi^+ p$ scattering,[23,24] which are $\omega_0^{++} = 1236 \pm 0.5$ MeV, $\Gamma_0^{++} = 120 \pm 1.6$ MeV.)

In the absence of detailed knowledge of the reaction amplitude it is conventional to assume that the resonance and accompanying particles are produced according to phase space. This procedure is usually adequate for a narrow resonance ($\Gamma_0 < 50$ MeV). In Table II we give the resonance parameters obtained by fitting the distributions with the product of the three-body phase space and $\Phi(\omega)$,[22] where $\Phi(\omega) = C \frac{\omega}{q} \frac{\omega_0 \Gamma(\omega)}{(\omega_0^2 - \omega^2)^2 + \omega_0^2 \Gamma^2(\omega)}$; C is a normalization constant.

When, as for N^*, the width Γ is energy-dependent, the peak position in the invariant-mass plot, ω_{peak}, falls below ω_0, the shift $\omega_0 - \omega_{peak}$ being proportional to Γ_0^2 (see Appendix B). In order to locate the actual

position of the peaks in the invariant-mass plots, we fitted them with an S-wave Breit-Wigner amplitude multiplied into phase space. This gives $\delta\omega_{peak} = 2.3 \pm 4.7$ MeV and $\delta\Gamma = 18 \pm 17$ MeV. Since the width of the ω^- distribution exceeds that of ω^{++}, one expects that $\delta\omega_0$ will be greater than $\delta\omega_{peak}$ when a P-wave Breit-Wigner form is used, and this is indeed the case.

Because reactions (1) and (2) are known to be dominated by one-pion exchange, the values obtained by OPE fit, $\delta\omega_0 = 7.9 \pm 6.8$ MeV and $\delta\Gamma_0 = 25 \pm 23$ MeV, are taken to be the best estimate of the resonance parameters. In fitting the data, we applied the χ^2 test with two parameters, ω_0 and Γ_0. Due to the energy dependence of the width, the errors in ω_0 and Γ_0 are correlated. Figures 19, 20 and 21 show the χ^2 distributions in two dimensions for ω_0 and Γ_0. The contour lines signify one standard deviation. The error matrix for the masses and widths in the OPE fit is given in Table III, and for the mass and width difference in Table IV. The correlation coefficient for the mass and width difference is 0.73.

(a)

24.75	20.36	16.84	14.10	12.02	10.54	9.58	9.07	8.97	9.23	1247
21.83	17.88	14.77	12.40	10.68	9.52	8.85	8.62	8.78	9.27	1246
19.21	15.69	12.98	10.98	9.59	8.74	8.36	8.40	8.81	9.53	1245
16.90	13.80	11.47	9.81	8.75	8.21	8.11	8.41	9.05	10.01	1244
14.90	12.20	10.24	8.93	8.18	7.92	8.09	8.64	9.52	10.69	1243
13.21	10.89	9.29	8.31	7.86	7.89	8.32	9.11	10.21	11.59	1242
11.82	9.88	8.62	7.96	7.80	8.10	8.78	9.80	11.13	12.70	1241
10.75	9.17	8.24	7.88	8.00	8.56	9.48	10.73	12.26	14.03	1240
9.99	8.75	8.14	8.07	8.46	9.27	10.42	11.88	13.61	15.57	1239
9.53	8.62	8.32	8.53	9.18	10.22	11.60	13.27	15.18	17.31	1238
9.38	8.80	8.78	9.26	10.16	11.43	13.02	14.88	16.97	19.27	1237
9.55	9.26	9.52	10.26	11.39	12.88	14.67	16.72	18.98	21.44	1236

130 135 140 145 150 155 160 165 170 175

Γ_o (MeV)

ω_o (MeV)

(b)

23.34	19.91	17.37	15.58	14.44	13.85	13.73	14.02	1238
21.05	18.04	15.88	14.44	13.61	13.31	13.46	14.00	1237
19.08	16.47	14.68	13.57	13.05	13.03	13.44	14.22	1236
17.43	15.21	13.77	12.98	12.75	13.00	13.15	14.66	1235
16.12	14.26	13.15	12.66	12.71	13.22	14.11	15.33	1234
15.13	13.62	12.82	12.62	12.94	13.69	14.80	16.23	1233
14.46	13.28	12.78	12.86	13.43	14.40	15.73	17.35	1232
14.11	13.24	13.03	13.37	14.18	15.37	16.90	18.70	1231
14.09	13.51	13.57	14.15	15.18	16.58	18.30	20.27	1230
14.38	14.08	14.39	15.21	16.45	18.04	19.93	22.07	1229

110 115 120 125 130 135 140 145

Γ_o (MeV)

ω_o (MeV)

Fig. 19

(a)

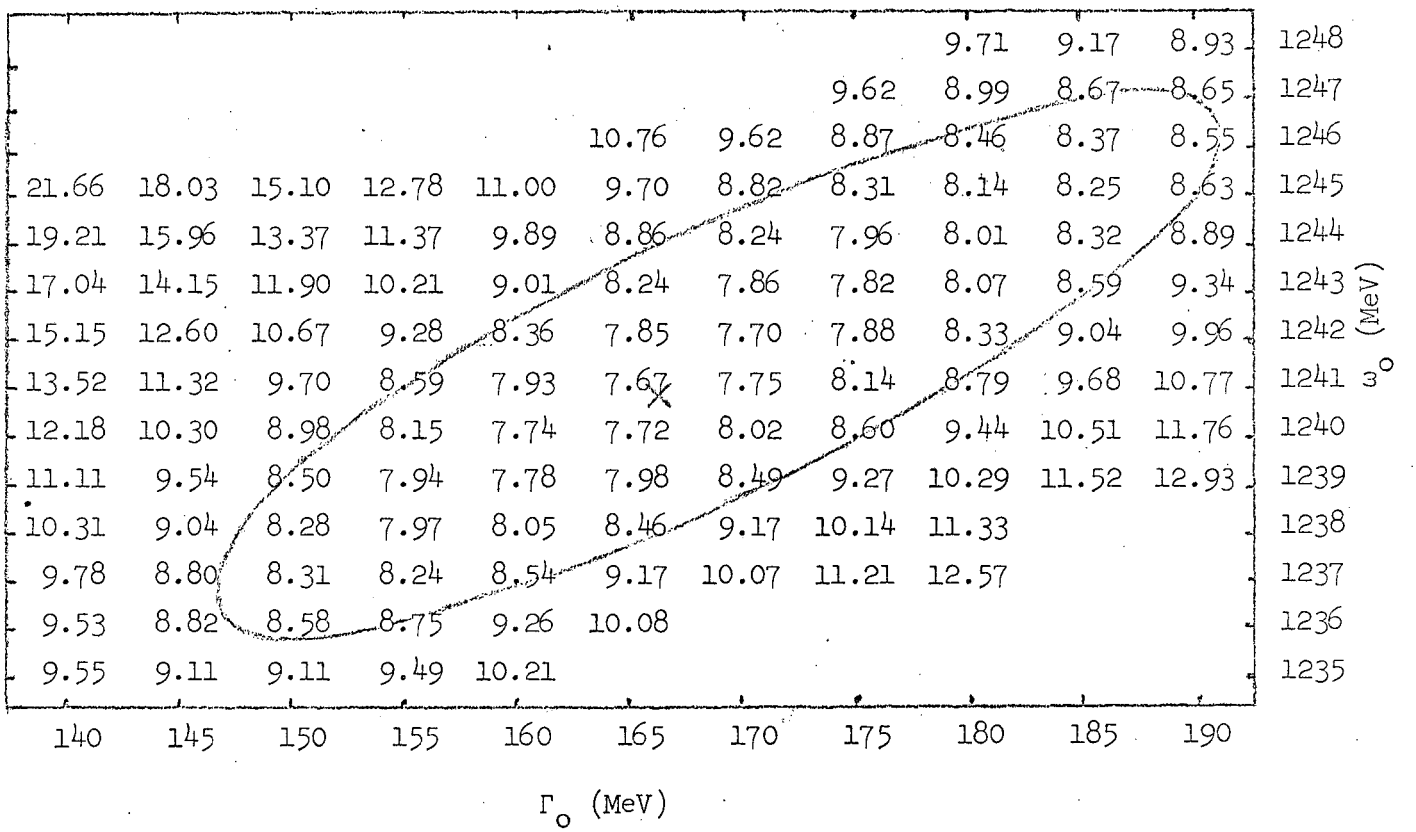
9.71 9.17 8.93 1248
9.62 8.99 8.67 8.65 1247
10.76 9.62 8.87 8.46 8.37 8.55 1246
21.66 18.03 15.10 12.78 11.00 9.70 8.82 8.31 8.14 8.25 8.63 1245
19.21 15.96 13.37 11.37 9.89 8.86 8.24 7.96 8.01 8.32 8.89 1244
17.04 14.15 11.90 10.21 9.01 8.24 7.86 7.82 8.07 8.59 9.34 1243
15.15 12.60 10.67 9.28 8.36 7.85 7.70 7.88 8.33 9.04 9.96 1242
13.52 11.32 9.70 8.59 7.93 7.67 7.75 8.14 8.79 9.68 10.77 1241
12.18 10.30 8.98 8.15 7.74 7.72 8.02 8.60 9.44 10.51 11.76 1240
11.11 9.54 8.50 7.94 7.78 7.98 8.49 9.27 10.29 11.52 12.93 1239
10.31 9.04 8.28 7.97 8.05 8.46 9.17 10.14 11.33 1238
9.78 8.80 8.31 8.24 8.54 9.17 10.07 11.21 12.57 1237
9.53 8.82 8.58 8.75 9.26 10.08 1236
9.55 9.11 9.11 9.49 10.21 1235
140 145 150 155 160 165 170 175 180 185 190
Γ_o (MeV)
ω_o (MeV)

(b)

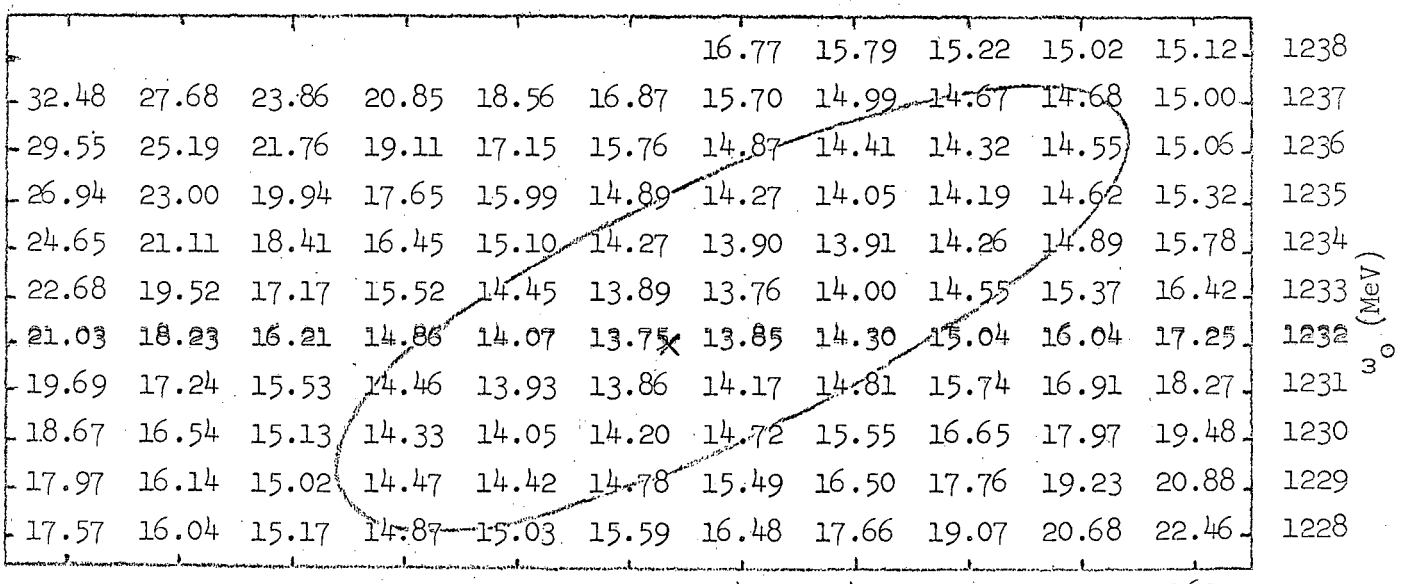
16.77 15.79 15.22 15.02 15.12 1238
32.48 27.68 23.86 20.85 18.56 16.87 15.70 14.99 14.67 14.68 15.00 1237
29.55 25.19 21.76 19.11 17.15 15.76 14.87 14.41 14.32 14.55 15.06 1236
26.94 23.00 19.94 17.65 15.99 14.89 14.27 14.05 14.19 14.62 15.32 1235
24.65 21.11 18.41 16.45 15.10 14.27 13.90 13.91 14.26 14.89 15.78 1234
22.68 19.52 17.17 15.52 14.45 13.89 13.76 14.00 14.55 15.37 16.42 1233
21.03 18.23 16.21 14.86 14.07 13.75 13.85 14.30 15.04 16.04 17.25 1232
19.69 17.24 15.53 14.46 13.93 13.86 14.17 14.81 15.74 16.91 18.27 1231
18.67 16.54 15.13 14.33 14.05 14.20 14.72 15.55 16.65 17.97 19.48 1230
17.97 16.14 15.02 14.47 14.42 14.78 15.49 16.50 17.76 19.23 20.88 1229
17.57 16.04 15.17 14.87 15.03 15.59 16.48 17.66 19.07 20.68 22.46 1228
110 115 120 125 130 135 140 145 150 155 160
Γ_o (MeV)
ω_o (MeV)

Fig. 20

(a)

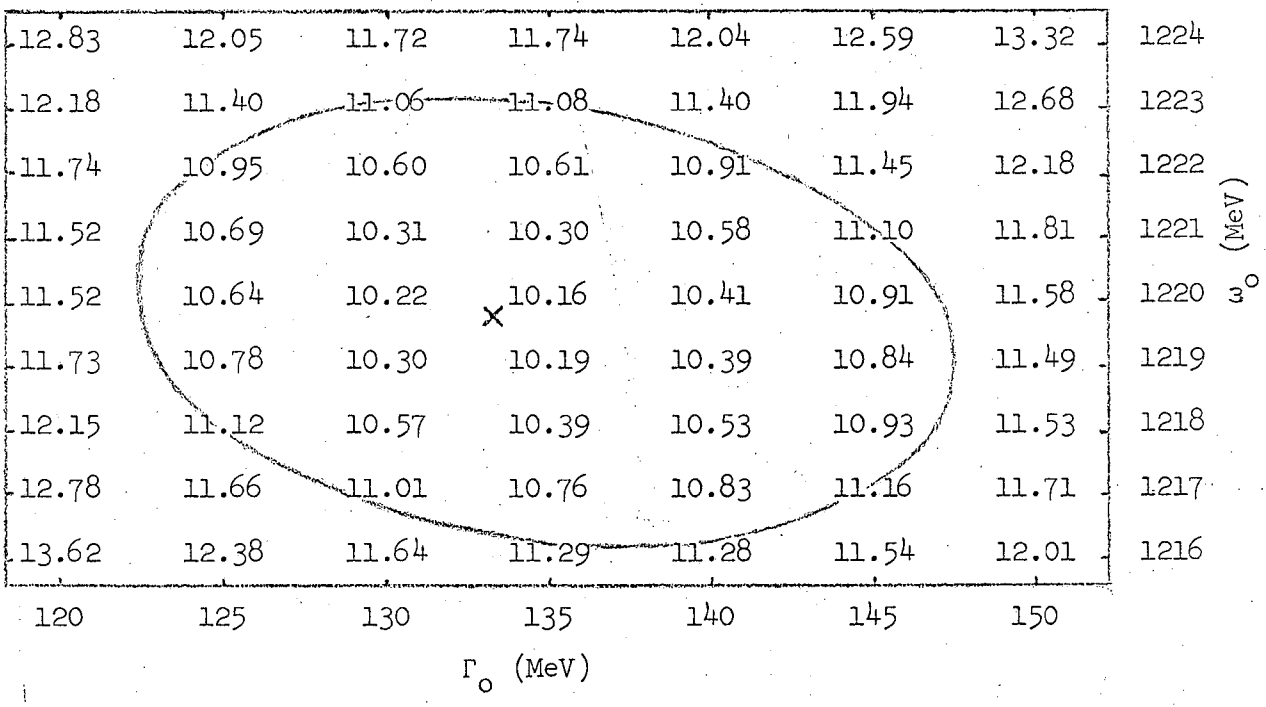
12.83 12.05 11.72 11.74 12.04 12.59 13.32 1224
12.18 11.40 11.06 11.08 11.40 11.94 12.68 1223
11.74 10.95 10.60 10.61 10.91 11.45 12.18 1222
11.52 10.69 10.31 10.30 10.58 11.10 11.81 1221
11.52 10.64 10.22 10.16 10.41 10.91 11.58 1220
11.73 10.78 10.30 10.19 10.39 10.84 11.49 1219
12.15 11.12 10.57 10.39 10.53 10.93 11.53 1218
12.78 11.66 11.01 10.76 10.83 11.16 11.71 1217
13.62 12.38 11.64 11.29 11.28 11.54 12.01 1216
120 125 130 135 140 145 150
Γ_o (MeV)
ω_o (MeV)

(b)

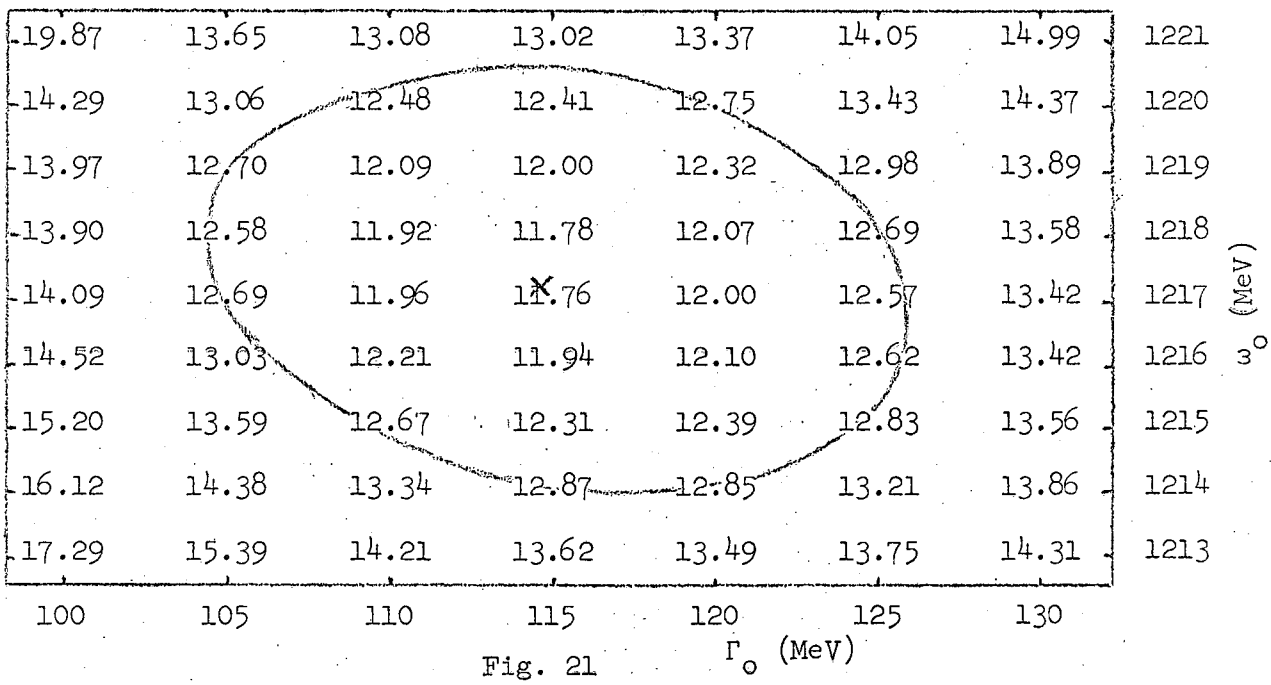
19.87 13.65 13.08 13.02 13.37 14.05 14.99 1221
14.29 13.06 12.48 12.41 12.75 13.43 14.37 1220
13.97 12.70 12.09 12.00 12.32 12.98 13.89 1219
13.90 12.58 11.92 11.78 12.07 12.69 13.58 1218
14.09 12.69 11.96 11.76 12.00 12.57 13.42 1217
14.52 13.03 12.21 11.94 12.10 12.62 13.42 1216
15.20 13.59 12.67 12.31 12.39 12.83 13.56 1215
16.12 14.38 13.34 12.87 12.85 13.21 13.86 1214
17.29 15.39 14.21 13.62 13.49 13.75 14.31 1213
100 105 110 115 120 125 130
Γ_o (MeV)
ω_o (MeV)

Fig. 21

VI. DISCUSSION

Within the $3/2^+$ decuplet, the following additional mass differences have been reported:

$$N^{*++} - N^{*o} = -0.45 \pm 0.85 \text{ MeV} \quad \text{(Ref. 24)}$$

$$Y^{*-} - Y^{*+} = 17 \pm 7 \text{ MeV} \quad \text{(Ref. 25)}$$

$$Y^{*-} - Y^{*+} = 4.3 \pm 2.2 \text{ MeV} \quad \text{(Ref. 26)}$$

$$\Xi^{*-} - \Xi^{*o} = 5.7 \pm 3.0 \text{ MeV} \quad \text{(Ref. 27)}$$

These values, together with the value obtained in our experiment, $\delta\omega_o = N^{*-} - N^{*++} = 7.9 \pm 6.8$ MeV, are compatible with the predictions of SU(3), SU(6), pure octet dominance (the tadpole model of Coleman and Glashow), and with the modified tadpole theory. In particular, the SU(6) scheme predicts $\delta\omega_o = N^{*-} - N^{*++} = 3\ (n-p) = 3.9$ MeV. The tadpole model of Coleman and Glashow predicts $\delta\omega_o = 3\ (N^{*+} - N^{*++}) = 3\ (\frac{\Sigma^+ - \Sigma^-}{N - \Xi})\ (N^* - Y^*) = 3\ (3.0) = 9.0$ MeV.[8] The modified tadpole theory, calculated by Socolow[9] gives $\delta\omega_o = 4.9$ MeV. He included the nontadpole terms due to the $N^* \gamma N$ vertices (self-energy diagram with a baryon octet member and a photon in the intermediate state) and $N^* \gamma N^*$ vertices (self-energy diagrams from the decuplet channel). The calculation of Dashen and Frautschi[10] within the framework of S-matrix theory gives $\delta\omega_o \leq 8.4$ MeV (using a similar method, Biswas, Bose and Pande[28] get $\delta\omega_o = 2.8$ MeV).

It is clear that our errors prevent us from distinguishing among theories with predictions in this range. The value predicted for $\delta\omega_o$ by using the measurements of Refs. 24 through 27 to evaluate the coefficients in $\Delta M = a + b\,Q + CQ^2$, predicted by SU(3) scheme,[7] is $\delta\omega_o = 4.8 \pm 3.3$ MeV. This, when combined with our direct measurement of 7.9 ± 6.8 MeV, yields $N^{*-} - N^{*++} = 5.4 \pm 3.0$ MeV.

ACKNOWLEDGMENTS

I would like to express my sincere appreciation and gratitude to Dr. Robert W. Birge and Professor Wilson M. Powell for their guidance and advice during the major part of my graduate studies.

I am indebted to Dr. George Gidal and Dr. Anne Kernan, who were my coworkers on several projects, for their help and advice on this experiment. In particular, I would like to express my gratitude to Dr. Anne Kernan for her aid throughout the course of this experiment. I am also indebted to Dr. Robert W. Birge and Dr. Robert Socolow for helpful discussions.

I would like to express my appreciation to Dr. Hildred Blewett, Dr. Hugh Brown, Dr. Ralph Shutt and the members of the Brookhaven National Laboratory's bubble chamber group along with the AGS operating crew, whose help made this experiment possible. I would also like to express my gratitude to Dr. Robert P. Ely and Dr. George E. Kalmus for their work during the bubble chamber run.

Many thanks are due the scanning and measuring staff of the Powell-Birge group and the staff of the Data Handling group under Mr. Howard S. White. I would also like to thank Mrs. Kathy Pierce for her secretarial task in preparation of this manuscript.

This work was done under the auspices of the U. S. Atomic Energy Commission.

APPENDICES

A. The Structure of the Deuteron and the Impulse Approximation

In the interaction of heavy nuclei, it is the collective behavior of the nucleons which is of primary importance rather than their individual properties. But this is not the case with the deuteron. The deuteron is rather special in that it consists of a single neutron loosely bound to a single proton. The two nucleons are separated by a relatively large distance, so that the incident particle probably interacts strongly with only one nucleon at a time. Recognizing these properties, G. F. Chew introduced the so-called Impulse Approximation to treat the problem of scattering on deuterons.[29]

In the Impulse Approximation the scattering amplitude for a complex nucleus is represented as a superposition of scattering amplitudes for free nucleons. It is based on the following assumptions:

(a) The range of the interacting forces is shorter than the average distance between two nucleons.

(b) The amplitude of the incident wave falling on each nucleon is approximately the same as if the nucleon were alone.

(c) Multiple scattering is negligible.

(d) The binding force has only the effect of giving to each nucleon a certain distribution of momentum.

The properties of the deuteron can be stated as follows:[30]

The deuteron is a rather diffuse, loosely bound structure with a binding energy of 2.226 MeV. Its spin is 1. The ground state is mainly an S-state, with a small admixture (~4%) of D-state. The momentum spectra of the nucleons in the S- and D-state are almost the same shape.

For most purposes, the presence of the D-state can be ignored. The $^3S_1$ ground state is well represented by Hulthén wave function

$$\psi_D(r) = N\,(e^{-\alpha r} - e^{-\beta r})/r\ ,$$

where $\alpha = 45.7$ MeV/$\hbar c$

$\beta = 7\alpha$

and $N = \left[\alpha\beta\,(\alpha+\beta)\,/\,2\pi\,(\beta-\alpha)^2\right]^{1/2}$ is the normalization constant. In momentum space, it is

$$\Phi_D(p) = \sqrt{\frac{2}{\pi}}\ N\hbar^{-3/2}\left[\frac{1}{(P/\hbar)^2+\alpha^2} - \frac{1}{(P/\hbar)^2+\beta^2}\right]$$

Figures 22 and 23 show the wave functions and their corresponding probabilities.

B. Shape and Position of a Resonance

The definition of precise masses of unstable resonant particles like N^*_{33} is not clear. Ordinarily we take the mass value where the phase-shift $\delta_{3,3}$ reaches 90°, or the cross-section is maximum, in the pion-nucleon scattering. We may alternately define the mass of the N^* to be the real part of the complex energy at the pole of the partial scattering amplitude. Experimentally, there is a problem of understanding why the N^*_{33}, for instance, appears at 1225 MeV in elastic scattering, at 1212 MeV in the invariant mass plot in a production reaction, and at 1238 MeV in the tables of particles.

To get the proper shape and position of a resonance in a production reaction, we consider the connection between the cross-sections for the production of a stable particle and an unstable one.[22] The two processes are shown in Fig. 24 . Let $d\sigma_S(\omega)$ be the cross-section for the produc-

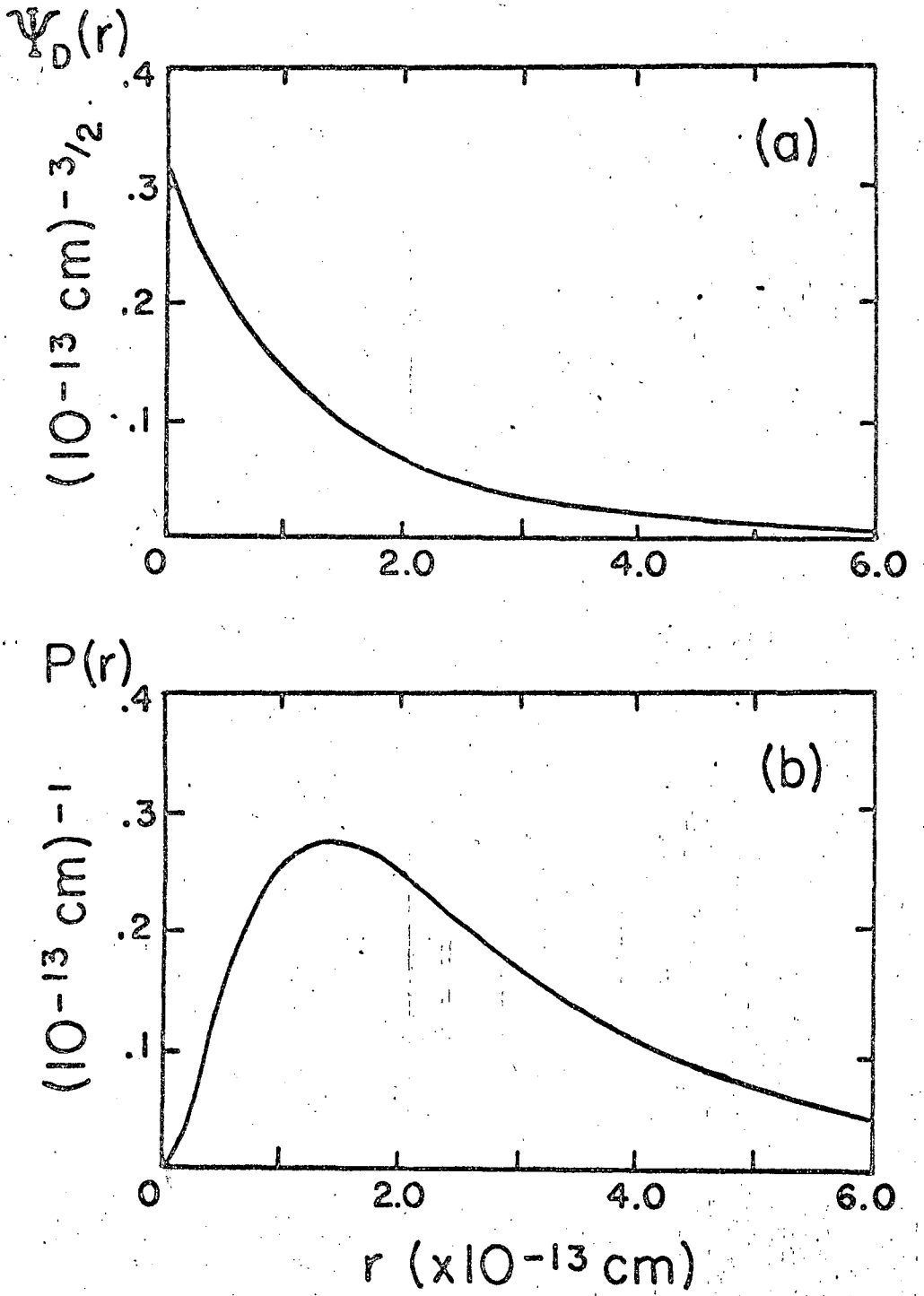
$\psi_D(r)$
$(10^{-13}\ cm)^{-3/2}$
.4
.3
.2
.1
(a)
0
2.0
4.0
6.0
P(r)
$(10^{-13}\ cm)^{-1}$
.4
.3
.2
.1
(b)
0
2.0
4.0
6.0
r ($\times 10^{-13}$ cm)

Fig. 22

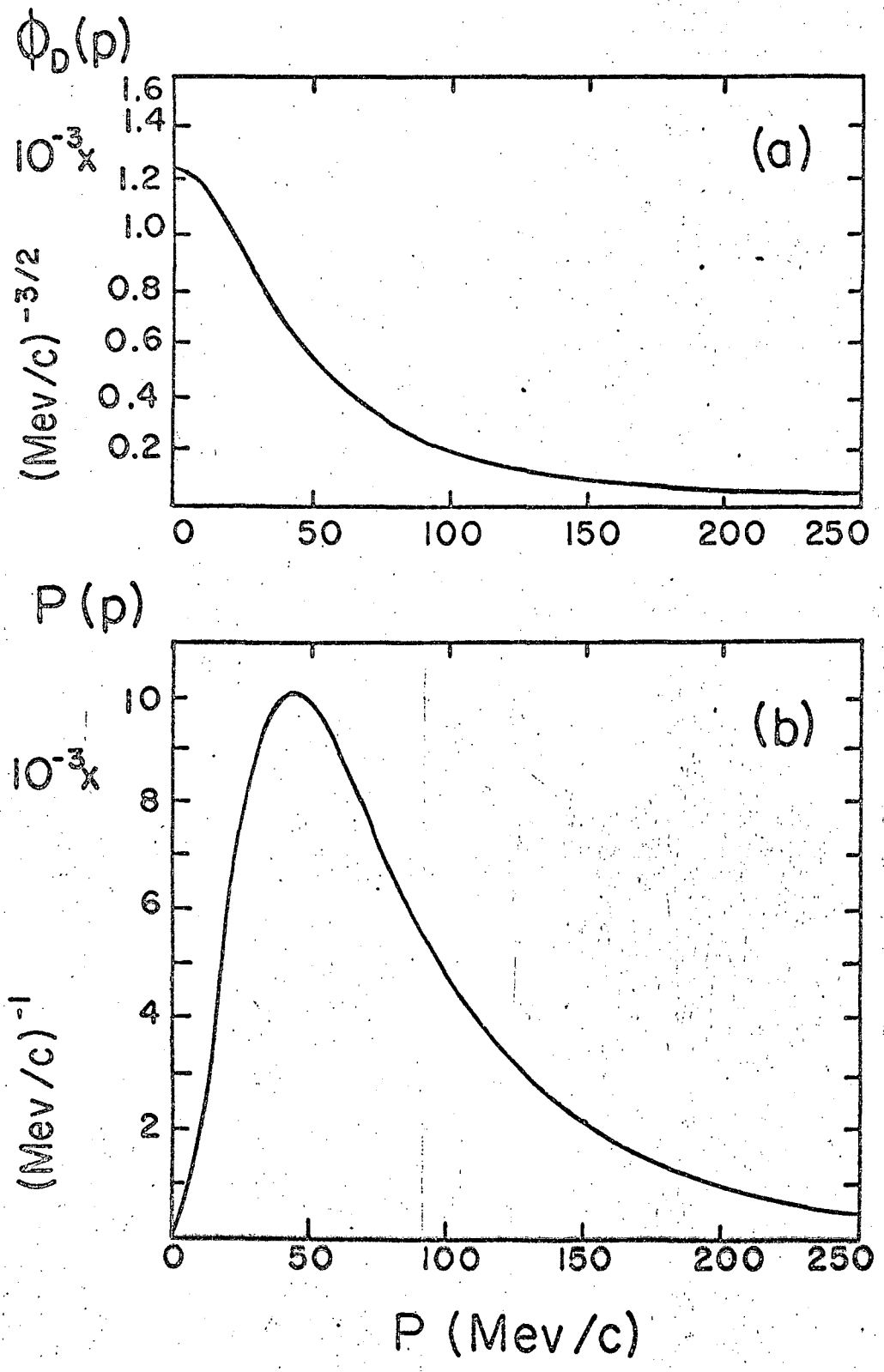
$\phi_D(p)$
10^{-3} x
$(Mev/c)^{-3/2}$
1.6
1.4
1.2
1.0
0.8
0.6
0.4
0.2
(a)
0
50
100
150
200
250
P(p)
10^{-3} x
$(Mev/c)^{-1}$
10
8
6
4
2
(b)
0
50
100
150
200
250
P (Mev/c)

Fig. 23

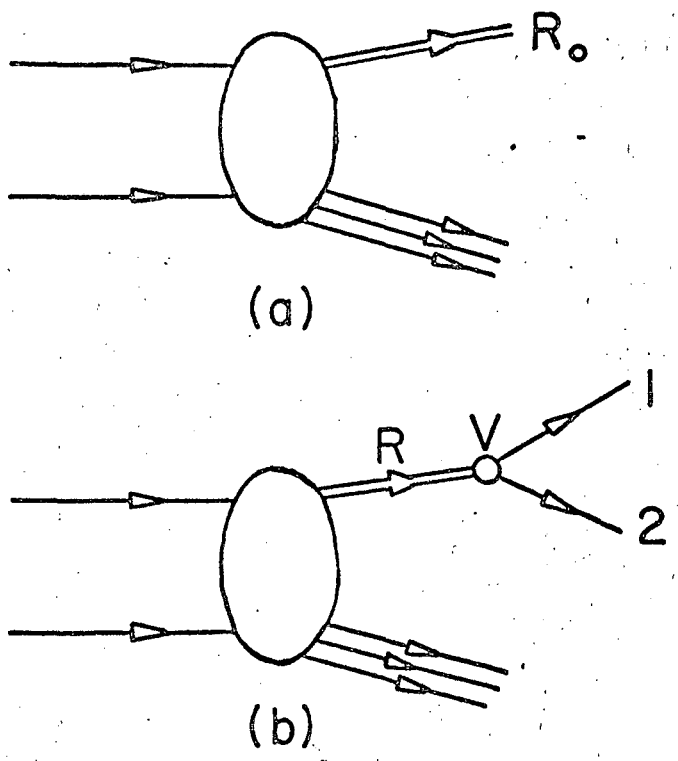

Fig. 24

tion of a stable particle Ro of mass ω, summed over the spin states of Ro. This process is represented by the diagram in Fig. 24(a). Then the cross-section for the production of the resonant state R, integrated over all angles of decay in the rest frame of the resonance, can be expressed in terms of $d\sigma_S(\omega)$ by modifying the calculation to include the decay vertex amplitude V for R and a propagator. This process is shown in Fig. 24(b). As a result, we obtain for the production cross-section of a resonance

$$d\sigma = d\sigma_S(\omega) \left[\frac{\pi^{-1} \omega_o \Gamma(\omega)}{(\omega_o^2 - \omega^2)^2 + \omega_o^2 \Gamma^2(\omega)} \right] d\omega^2,$$

where ω_o is the mass of the resonance, and $\Gamma(\omega)$ is the width, defined[22] as

$$\Gamma(\omega) = \frac{1}{32\pi^3} \frac{1}{(2J+1)} \sum \int |V|^2 \frac{q}{\omega} d\Omega_{12}.$$

Here J is the angular momentum of the resonant state. The summation is over the spins of the outgoing decaying particles and the integration is over the decay angles of the two-body phase space, f, defined below.

If we assume that a stable particle and the (n-1) particles are produced according to the phase space, $d\sigma_S(\omega)$ will be proportional to the (n-1) body phase space. The n body phase space, dF_n, can be written in terms of (n-1) body phase space, dF_{n-1}, as follows:

$$dF_n = \int \frac{d^3 P_1 \, d^3 P_2 \ldots d^3 P_n}{(2\pi)^{3n} (2E_1)(2E_2)\ldots(2E_n)} \delta^4 (P_1 + P_2 + \ldots P_n - P)$$

$$dF_n = \int \frac{d^3 Q \, d^3 P_3 \ldots d^3 P_n}{(2\pi)^{3(n-1)} (2Q_o)(2E_3)\ldots(2E_n)} \delta^4 (Q + P_3 + \ldots P_n - P)$$

$$= f dF_{n-1},$$

where $$f = \frac{1}{4(2\pi)^3} \frac{q}{\omega} d\Omega_{12} \, d\omega^2$$

is the two-body phase space in the rest frame of particles 1 and 2, and $Q = P_1 + P_2$. We then have

$$d\sigma = C \left[\frac{\pi^{-1} \omega_o \Gamma(\omega)}{(\omega_o^2 - \omega^2)^2 + \omega_o^2 \Gamma^2(\omega)} \right] dF_{n-1} d\omega^2 = C' \left[\frac{\omega_o \Gamma(\omega)}{(\omega_o^2 - \omega^2)^2 + \omega_o^2 \Gamma(\omega)} \right] \frac{\omega}{q} dF_n,$$

where C's are the normalization constants. With this formula, the apparent peak position in the invariant mass plot is given by

$$\frac{\omega_o - \omega_{peak}}{\Gamma_o} \simeq \frac{2\ell + 1}{8} \left(\frac{\Gamma_o}{\omega_o}\right) \left[\frac{\omega_o^4 - (m_1^2 - m_2^2)^2}{\omega_o^4 - 2 (m_1^2 + m_2^2) \omega_o^2 + (m_1^2 - m_2^2)^2} \right],$$

if $\Gamma(\omega) \simeq \Gamma_o (q/q_o)^{2\ell+1}$.[22] The factor in the square brackets is $\omega_o^2 (dq^2/d\omega^2)_o / q_o^2$. (According to this formula, the peak position of N^* with $\omega_o = 1238$ MeV and $\Gamma_o = 125$ MeV appears at about 1215 MeV.)

C. Off-the-Mass-Shell Corrections in the One-Pion-Exchange Model

Since the exchanged pion in the OPE (one-pion-exchange) model is virtual, in the physical region off-the-mass-shell effects enter. To relate the virtual cross-section to the physical cross-section, we consider in detail the coupling of the incoming nucleon and the virtual π to the N^* (Fig. 25). At this vertex the matrix element in the rest frame of N^* is proportional to

$$u_2 (\underset{\sim}{p}_N - \underset{\sim}{p}_\Delta)_j \left[\delta_{jk} - \frac{1}{3} \sigma_j \sigma_k\right] \epsilon_k u_1,$$

where u_1 and u_2 are the N^* and proton spinors, respectively, $(\underset{\sim}{p}_N - \underset{\sim}{p}_\Delta)$ represents the relative momenta of the incident nucleon and the virtual pion, the term in brackets is the spin -3/2 projection operator, and ϵ_k is the N^* polarization vector. The transition probability is then proportional to

$$(p^{off})^2 \left[(\omega + m_N)^2 + \Delta^2 \right],$$

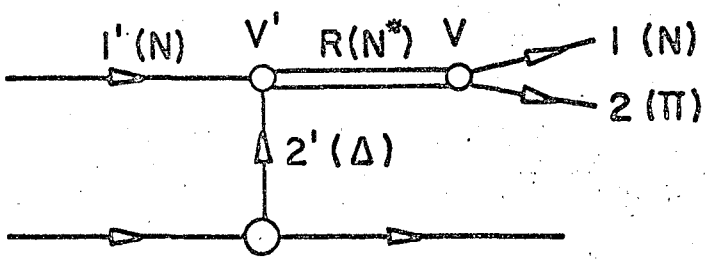

Fig. 25

where $$(p^{off})^2 = \frac{\left[(\omega + m_N)^2 + \Delta^2\right]\left[(\omega - m_N)^2 + \Delta^2\right]}{4\,\omega^2}$$

is the three-momentum squared of the incident particle, and Δ^2 is the four-momentum transfer squared.

Now the cross-section

$$d\sigma = d\sigma_S(\omega)\ \frac{\pi^{-1}\,\omega_o\,\Gamma\,(\omega)}{(\omega_o^2 - \omega^2)^2 + \omega_o^2\,\Gamma^2\,(\omega)}\ d\omega^2$$

can be written as

$$d\sigma = d\sigma_S(\omega)\ \frac{\sin^2\delta}{\pi\,\omega_o\,\Gamma\,(\omega)}\ d\omega^2,$$

where δ is the resonant phase shift given by

$$\tan\delta = \frac{\omega_o\ \Gamma\,(\omega)}{\omega_o^2 - \omega^2}$$

Here $d\sigma_S$ is proportional to $(p^{off})^2\,((\omega + m_N)^2 + \Delta^2)$. And

$$\Gamma\,(\omega) = \Gamma_o\,(q/q_o)^3\left[\frac{(\omega + m_N)^2 - m_\pi^2}{\omega^2}\right]\left[\frac{(\omega_o + m_N)^2 - m_\pi^2}{\omega_o^2}\right]^{-1},$$

where q is the three-momentum of the pion in the N^* rest system.[22]

Therefore,

$$d\sigma \propto \frac{(p^{off})^2}{q^3}\ \frac{\left[(\omega + m_N)^2 + \Delta^2\right]\ \omega^2}{\left[(\omega + m_N)^2 - m_\pi^2\right]}\ \sin^2\delta\, d\omega^2\ .$$

Comparing this with the factor from the pole-approximation of Chew and Low,

$$q\,\sigma_{scatt}(\omega) \propto \frac{\sin^2\delta}{q}\ ,$$

we obtain the so-called off-the-mass-shell correction[22]

$$\frac{d\sigma}{d\sigma_{pole}} = \frac{(p^{off})^2}{q^2}\ \frac{\left[(\omega + m_N)^2 + \Delta^2\right]}{\left[(\omega + m_N)^2 - m_\pi^2\right]} = \frac{\left[(\omega + m_N)^2 + \Delta^2\right]^2\left[(\omega - m_N)^2 + \Delta^2\right]}{\left[(\omega + m_N)^2 - m_\pi^2\right]^2\left[(\omega - m_N)^2 - m_\pi^2\right]}\ .$$

This correction factor is kinematic in origin, whereas the empirical

form factor of Ferrari and Selleri[20] represents the dynamical modification of the vertices and propagator. The explicit form of $d\sigma$ pole may be written as

$$d\sigma_{\text{pole}} = \frac{f^2\,\omega}{2\pi\, p_i^2\, m_\pi^2}\left[\omega^4 - 2\omega^2\,(m_N^2 + m_\pi^2) + (m_N^2 - m_\pi^2)^2\right]^{\frac{1}{2}}\ \frac{\Delta^2}{(\Delta^2 + m_\pi^2)^2}\ \sigma_{\pi N}(\omega)\, d\Delta^2 d\omega$$

where $\sigma_{\pi N}(\omega) = \frac{8\pi}{q^2}\ \frac{\omega_o^2\,\Gamma(\omega)}{(\omega_o^2 - \omega^2)^2 + \omega_o^2\,\Gamma^2(\omega)}$

is the Breit-Wigner formula for πN scattering, q is the pion momentum in the πN rest frame, and p_i is the laboratory momentum of the incident nucleon.

Table I. Tadpole and nontadpole contribution to the electromagnetic mass differences.

Mass Difference	A[(a)]	B[(b)]	C[(c)]
$N^{*++} - N^{*+}$	-3.0	0.2	4.4
$N^{*++} - N^{*o}$	-6.1	-2.9	2.7
$N^{*++} - N^{*-}$	-9.1	-9.1	-4.9
$Y^{*+} - Y^{*o}$	-3.0	-2.8	-1.4
$Y^{*+} - Y^{*-}$	-6.1	-9.1	-9.1
$Y^{*o} - Y^{*-}$	-3.0	-6.2	-7.6
$\Xi^{*o} - \Xi^{*-}$	-3.0	-6.3	-7.7

(a) A is the tadpole term alone.

(b) B is the tadpole term plus the self-energy diagrams with a baryon octet member and a photon in the intermediate state (see Ref. 9, p. 95).

(c) C comprises B plus an estimate of the contribution of the self-energy diagrams from the decuplet channel (see Ref. 9, p. 102).

Table II. Masses, widths, and mass differences for N^* (all in MeV).

	With P-wave Breit-Wigner amplitude.		With S-wave Breit-Wigner amplitude
	OPE	Phase Space	Phase Space
Mass ω_0 N^{*-}	1241.3 ± 5.1	1240.7 ± 5.1	1219.7 ± 3.4
N^{*++}	1233.4 ± 4.4	1232.0 ± 4.9	1217.4 ± 3.2
Reduced-width Γ_0 N^{*-}	149 ± 18	166 ± 21	133 ± 13
N^{*++}	124 ± 14	137 ± 17	115 ± 11
Mass difference $\delta\omega_0$	7.9 ± 6.8	8.7 ± 7.8	2.3 ± 4.7
Width difference $\delta\Gamma_0$	25 ± 23	29 ± 27	18 ± 17

Table III. Error Matrix for masses and widths in the OPE fit [all in $(\text{MeV})^2$].

	ω_0^-	Γ_0^-	ω_0^{++}	Γ_0^{++}
ω_0^-	26.2	69.6	.0	.0
Γ_0^-	69.6	326.	.0	.0
ω_0^{++}	.0	.0	19.7	43.9
Γ_0^{++}	.0	.0	43.9	201.

Table IV. Error Matrix for mass and width differences in the OPE fit [all in $(\text{MeV})^2$].

	$\delta\omega_0$	$\delta\Gamma_0$
$\delta\omega_0$	45.9	113.
$\delta\Gamma_0$	113.	527.

FOOTNOTES AND REFERENCES

1. H. Anderson, E. Fermi, R. Martin and D. Nagle, Phys. Rev. 91, 155 (1953).

2. M. Gell-Mann, Phys. Rev. 125, 1067 (1962); S. Okubo, Progr. Theoret. Phys. (Kyoto) 27, 949 (1962).

3. S. Okubo, J. Phys. Soc. Japan 19, 1507 (1964).

4. C. Becchi, E. Eberle and G. Morpurgo, Phys. Rev. 136, B808 (1964).

5. S. Coleman and S. L. Glashow, Phys. Rev. Letters 6, 423 (1961).

6. D. Carmony, G. Pjerrou, P. Schlein, W. Slater, D. Stork and H. Ticho, Phys. Rev. Letters 12, 482 (1964), and other recent data cited therein; L. Jauneau, D. Morellet, U. Nguyen-Khac, et al., Phys. Letters 4, 49 (1963).

7. S. P. Rosen, Phys. Rev. Letters 11, 100 (1963); A. J. MacFarlane and E. C. G. Sudarshan, Nuovo Cimento 31, 1176 (1964).

8. S. Coleman and S. L. Glashow, Phys. Rev. 134, B671 (1964).

9. R. Socolow, Electromagnetic Masses in the Unitary Symmetry Theory (Ph.D. Thesis), Harvard University, May 1964 (unpublished).

10. R. Dashen and S. Frautschi, Phys. Rev. Letters 13, 497 (1964) and Phys. Rev. 137, B1331 (1965).

11. F. Gürsey and L. A. Radicati, Phys. Rev. Letters 13, 173 (1964); A. Pais, Phys. Rev. Letters 13, 175 (1964); B. Sakita, Phys. Rev. 136, B1756 (1964).

12. T. K. Kuo and Tsu Yao, Phys. Rev. Letters 14, 79 (1965).

13. C. Baltay, J. Sandweiss, J. Sanford, H. Brown, M. Webster and S. Yamamoto, The Separated Beam at the AGS--Performance with Antiprotons and π^+ Mesons, in Proceedings of the 1962 Conference on Instrumentation for High Energy Physics, CERN, 1962 (North Holland Publishing

Co., Amsterdam, Holland, 1962); J. Leitner, G. Moneti and N. P. Samios, Performance of the AGS Separated Beam with High Energy Kaons, op. cit.

14. R. I. Louttit, in Proceedings of the 1960 Conference on Instrumentation for High Energy Physics (Lawrence Radiation Laboratory, Berkeley, California), p. 117.

15. F. T. Solmitz and S. G. Wojcicki, "Missing Mass Calculations", Physics Note No. 367, Lawrence Radiation Laboratory, University of California (1962).

16. FOG and CLOUDYFAIR Data-Processing-System Reference Manuals, Lawrence Radiation Laboratory Document UCID-1340, March 1961 (unpublished).

17. A. P. Batson, B. B. Culwick, H. B. Klepp and L. Riddiford, Proc. Roy. Soc. (London) A, 251, 233 (1959).

18. R. Birge, R. Ely, G. Gidal, G. Kalmus, A. Kernan and S. Kim, The Reaction $n + n \rightarrow n + p + \pi^-$ at 1.9 GeV/c, Lawrence Radiation Laboratory Report UCRL-11550, July 1964 (unpublished).

19. D. V. Bugg, A. J. Oxley, J. A. Zoll, J. G. Rushbrooke, V. E. Barnes, J. B. Kinson, W. P. Dodd, G. A. Doran and L. Riddiford, Phys. Rev. 133, B1017 (1964).

20. E. Ferrari and F. Selleri, Phys. Rev. Letters 7, 387 (1961); E. Ferrari and F. Selleri, Nuovo Cimento 27, 1450 (1963).

21. G. F. Chew and F. E. Low, Phys. Rev. 113, 1644 (1959).

22. J. D. Jackson, Nuovo Cimento 34, 1644 (1964).

23. N. Klepikov, V. Meshcheryakov and S. Sokolov, Joint Institute for Nuclear Research (Dubna) Report JINR-D-584 (1960).

24. M. G. Olsson, Phys. Rev. Letters 14, 118 (1965).

25. W. A. Cooper, H. Filthuth, A. Fridman, E. Malamud, E. S. Gelsema, J. C. Kluyver and A. G. Tenner, Phys. Letters 8, 365 (1964).

26. D. O. Huwe, Study of the Reaction $K^- p \rightarrow \pi^+ \pi^-$ from 1.2 to 1.7 BeV/c (Ph.D. Thesis), Lawrence Radiation Laboratory Report UCRL-11291, July 1964 (unpublished).

27. G. M. Pjerrou, P. E. Schlein, W. E. Slater, L. T. Smith, D. H. Stork, and H. K. Ticho, Phys. Rev. Letters 14, 275 (1965).

28. S. N. Biswas, S. K. Bose, and L. K. Pande, Phys. Rev. 138, B163 (1965).

29. G. F. Chew, Phys. Rev. 80, 196 (1950).

30. L. Hulthén and M. Sugawara, Handbuch der Physik 39, Spring-Verlag, Berlin (1957).

FIGURE CAPTIONS

Fig. 1: (a) Baryon octet.

(b) Baryon decuplt.

Fig. 2: Schematic diagram of the beam.

Fig. 3: Distribution of 1/P Beam, where P Beam is the beam deuteron momentum.

Fig. 4: Mass-squared distribution of the final state neutron in $n\ n \rightarrow p\ n\ \pi^-$.

Fig. 5: Assumed beam proton momentum distribution in reaction, $p\ p \rightarrow n\ p\ \pi^+$. (This is obtained by transforming the Hulthén distribution in momentum space from beam rest system to the laboratory system.)

Fig. 6: χ^2 distribution in reactions (a) $D\ n \rightarrow p_S^B\ p\ n\ \pi^-$, and (b) $p\ p \rightarrow n\ p\ \pi^+$.

Fig. 7: Errors in the effective masses, (a) $\omega\ \pi^-\ n$ and (b) $\omega\ \pi^+\ p$.

Fig. 8: Distribution in transverse momentum, P_{TRAN}, of spectator nucleons in the beam deuterons. The smooth curve is the Hulthén wave function in momentum space, folded into the transverse plane.

Fig. 9: The $(\pi^-\ n)$ invariant-mass distribution in the reaction $d\ n \rightarrow n_S^B\ p\ p\ \pi^-$, where n_S^B is a spectator neutron in the beam deuteron.

Fig. 10: Invariant-mass distributions, (a) ω_{23} and (b) ω_{13}, in $n\ n \rightarrow p_1\ n_2\ \pi_3^-$.

Fig. 11: Invariant-mass distributions of $(\pi^-\ n)$ and $(\pi^+\ p)$ in the reactions $n\ n \rightarrow n\ p\ \pi^-$ and $p\ p \rightarrow n\ p\ \pi^+$. The $(\pi^+\ p)$ distribution (558 events) has been normalized to the area of the $(\pi^-\ n)$ distribution (695 events).

Fig. 12: Inverse momentum distribution of "no-field" tracks taken with the magnetic field turned off.

Fig. 13: Assumed C. M. energy distribution. Dotted curve corresponds to $n\ n \rightarrow p\ n\ \pi^-$ and the solid curve is for $p\ p \rightarrow n\ p\ \pi^+$. (These are obtained using the Hulthén deuteron wave functions.)

Fig. 14: (a) Normalized momentum distributions for π^- and π^+ in the reactions $n\ n \rightarrow p n \pi^-$ and $p\ p \rightarrow n\ p\ \pi^+$, respectively.

(b) Normalized momentum distributions for neutrons and protons in the reactions $n\ n \rightarrow p\ n\ \pi^-$ and $p\ p \rightarrow n\ p\ \pi^+$, respectively.

Fig. 15: Center-of-mass angular distributions of (a) protons, and (b) neutrons in $n\ n \rightarrow p\ n\ \pi^-$. The dotted lines are (a) neutrons and (b) protons in $p\ p \rightarrow n\ p\ \pi^+$ (at 970 MeV).[19]

Fig. 16: Diagrams for One-Pion Exchange.

n_1 stands for incident nucleon.

n_2 is target nucleon.

π^- is the outgoing π, n is the outgoing neutron, and P is the outgoing proton in $n\ n \rightarrow p\ n\ \pi^-$.

Fig. 17: Proton kinetic-energy spectrum in the laboratory. The smooth curve is the distribution predicted by the Ferrari and Selleri OPE model, using the form factor which gives a best fit to the p-p data (at 970 MeV).[19]

Fig. 18: Total C. M. energy distribution. (This corresponds to the distribution in the reaction energies.)

Fig. 19: χ^2 distribution with 15 degrees of freedom fitted with OPE formula [Eq.(3)] for (a) N^{*-} and (b) N^{*++}.

Fig. 20: χ^2 distribution with 15 degrees of freedom fitted with the formula with the constant matrix element [Eq.(4)] for (a) N^{*-}

and (b) N^{*++}.

Fig. 21: χ^2 distribution with 15 degrees of freedom fitted with the S-wave Breit-Wigner formula multiplied by the three-body phase space for (a) N^{*-} and (b) N^{*++}.

Fig. 22: (a) Deuteron wave function $\psi_D(r) = N \frac{e^{-\alpha r} - e^{-\beta r}}{r}$.

(b) Probability of two nucleons being separated by a distance between r and r + dr.

Fig. 23: (a) Deuteron wave function in momentum space.

(b) Probability of nucleons being between p and p + dp.

Fig. 24: (a) Diagram for production of a stable particle, R_o.

(b) Diagram for production of an unstable resonance, R.

Fig. 25: Diagram for exchange of a (virtual) pion in the intermediate state.